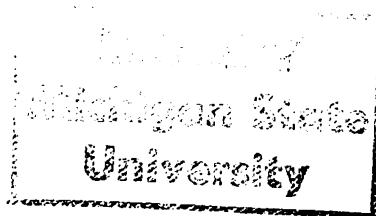




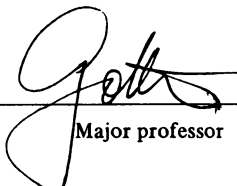
113  
972  
THS



This is to certify that the  
thesis entitled

A STUDY OF ROLLING AND RECRYSTALLIZATION  
TEXTURES IN Cu - 5 % Ag  
presented by  
Wonjoon Kim

has been accepted towards fulfillment  
of the requirements for  
m.s. degree in materials science

  
Major professor

Date 2/21/86



RETURNING MATERIALS:

Place in book drop to  
remove this checkout from  
your record. FINES will  
be charged if book is  
returned after the date  
stamped below.

--	--	--

A STUDY OF ROLLING AND RECRYSTALLIZATION TEXTURES IN Cu--5%Ag

By

Wonjoong Kim

A DISSERTATION

Submitted To

MICHIGAN STATE UNIVERSITY

in partial fulfilment of the requirements

for the degree of

MASTER OF SCIENCE

Department of Metallurgy, Mechanics

and Materials Science

1986

## ABSTRACT

### A STUDY OF ROLLING AND RECRYSTALLIZATION TEXTURES IN Cu-5%Ag

By

Wonjoong Kim

The rolling and recrystallization texture of Cu-5%Ag were obtained from both (111) and (200) reflections by using the Schuoz refoection method. Complete pole figures were then obtained by normaling all data with respect to the random powder specimen. For the rolling textures the transition observed for both the Cu-5%Ag solid solution alloy and the two phase alloy is similar to that observed in the brass and Cu-P alloy. For the recrystallization textures, however, both the Cu-Ag solid solution alloy and the Cu-Ag two phase alloy didn't show brass recrystallization textures. While the recrystallization textures of the Cu-Ag solid solution annealed at 600°C revealed a goss component in addition to the cube- and {258}<121> component present at 550°C the recrystallization textures of the Cu-Ag two phase alloy were composed of the goss- and {258}<121> component.

## ACKNOWLEDGEMENTS

I would like to express my deep sense of gratitude to Professor Gunter Gottstein for his constant guidance and encouragement during the course of this research. I would also like to thank my colleagues Dongteak Chung, Chulsoo Kim, and Wookwhan Sur for their help and encouragement all through this project.

I extend special thanks to my family for their encouragement during my period of study. Finally I would like to thank the Department of Energy for providing the fund for this research.

## TABLE OF CONTENTS

<u>Chapter</u>	<u>Page</u>
LIST OF FIGURES . . . . .	<b>iv</b>
1. INTRODUCTION . . . . .	1
2. REVIEW OF PREVIOUS STUDY . . . . .	2
2.1 Rolling Textues of fcc Metals and Alloys . . . . .	2
2.2 Theories of Rolling Texture Transition . . . . .	8
2.3 Annealing Textures of fcc Metals and Alloys . . . . .	12
2.4 Theories of the Development of Recrystallization Texture . . . . .	15
3. EXPERIMENTAL PROCEDURE AND TECHNIQUES . . . . .	18
3.1 Pole Figure System . . . . .	18
3.1.1 Principles of X-ray Texture Goniometers . . . . .	18
3.1.2 POle Figure Projections . . . . .	19
3.1.3 Installation of Pole Figure System . . . . .	21
3.1.4 Software System . . . . .	24
3.1.5 Operation of System . . . . .	28
3.2 Specimen Preparation . . . . .	29
3.2.1 Rolling Process of Cu-5%Ag . . . . .	29
3.2.2 Heat Treatment of the samples . . . . .	32
4. RESULTS AND DISCUSSION . . . . .	34
4.1 Rolling Texture . . . . .	34
4.1.1 Exper imental Results . . . . .	34
4.1.2 Discussion . . . . .	34
4.2 Recrystallization Texture . . . . .	35
4.2.1 Exper imental Results . . . . .	35

4.2.2	Discussion . . . . .	35
5	Summary and Conclusions . . . . .	42



## LIST OF FIGURES

<u>Figure No.</u>		<u>Page</u>
1	Positions of the $\langle 111 \rangle, \langle 100 \rangle$ poles of some components of the texture . . . . .	3
2	(111) pole figures for Cu and $\alpha$ -brass after rolling at room temperature . . . . .	7
3	(111) pole figures obtained for Cu after rolling at different temperatures . . . . .	7
4	Shear misfit produced by the three different shear components  (a) Taylor case, (b) misfit in $\epsilon_{xz}$ , (c) misfit in $\epsilon_{xy}$ , and (d) misfit in $\epsilon_{yz}$ . . . . .	9
5	Orientation distribution along the skeleton line as calculated for $\{111\} \langle 110 \rangle$ slip according to the theory of relaxed constraints if (a) $\epsilon_{xz}$ (b) $\epsilon_{xy}$ (c) $\epsilon_{yz}$ (d) $\epsilon_{xz}$ and $\epsilon_{xy}$ (e) all shear strains are assumed to be unconstrained . . . . .	10
6	(111) pole figures of a $\alpha$ -brass single crystal after unconstrained rolling ( $\alpha$ ) and after rolling with constraints on $\epsilon_{yz}$ ( $\beta$ ), which leads to twinning on the (111) plane perpendicular to TD (b) Schematic of the shape change of the initially rectangular rolling plane of the crystal. (c) $\tan \alpha$ as a function of the thickness reduction for the cases of	

16 Pole figure system configuration. . . . .	25
17 (111) pole figures of a lithium fluoride single crystal and an aluminum single crystal. . . . .	26
18 Pole figure software system configuration. . . . .	27
19 Hardness variation during annealing of rolled specimens. . . . .	33
20 (111),(200) pole figures for Cu-5%Ag (solid solution) rolled to 95% reduction at room temperature. . . . .	37
21 (111),(200) pole figures for Cu-5%Ag (two phase alloy) rolled to 95% reduction at room temperature. . . . .	38
22-1 (111),(200) pole figures of recrystallization textures of Cu-5%Ag solid solution alloy after rolling and annealing at 550°C. . . . .	39
22-2 (111),(200) pole figures of recrystallization textures of Cu-5%Ag solid solution alloy after rolling and annealing at 600°C. . . . .	40
23 (111),(200) pole figures of recrystallization textures of Cu-5%Ag two phase alloy after rolling and annealing at 600°C. . . . .	41

unconstrained ( $\alpha$ ) and constrained ( $\beta$ ) deformation . . . . .	11
7 (111) pole figures of rolling textures of Cu-Zn alloys before and after recrystallization. (a),(c),and (e) subsequent to rolling with 95% thickness reduction of (a)Cu and(c)Cu-5%Zn at room temperature and (e) Cu-5% Zn at 77 <sup>0</sup> K. (b),(d), and (f) show the corresponding textures after primary recrystallization. . . . .	14
8 40 <sup>0</sup> <111> rotations of both components of the (011)[211] orientation.	16
9 39 <sup>0</sup> <110> rotations of both components of the (011)[211] orientation.	16
10 A sheet sample mounted in back-reflection position. . . . .	20
11 Starting position of the sample. . . . .	20
12 The diffraction vector d is brought into the sample direction $\{\alpha,\beta\}$ by the rotations $\phi$ and $\phi_1$ . . . . .	22
13 Geometric illustration of axial motion. . . . .	22
14 The illustration of pole figure projection. . . . .	23
15 The two dimensional illustration of pole figure projection. . . . .	23

## CHAPTER 1

### INTRODUCTION

The rolling textures as well as the recrystallization textures in fcc alloys as function of the composition has been the subject of several investigations,(1). Most of these investigations are based on the analysis of pole figures. This method led to an approximation of the rolling textures by the three ideal orientations  $\{011\} \langle 211 \rangle$ ,  $\{123\} \langle 634 \rangle$ , and  $\{112\} \langle 111 \rangle$  in the case of pure copper and by the two orientations  $\{011\} \langle 211 \rangle$  and  $\{011\} \langle 100 \rangle$  in the case of  $\alpha$  brass with high Zn-content. After primary recrystallization, in the first case the cube orientation and in the second case the brass recrystallization orientation was observed,(1). For the intermediate Zn-content the rolling textures were found to give a continuous transition from one to the other. For the corresponding recrystallization texture, however, discontinuous, much more complicated transition was found with several components to newly occur and to disappear which seemed to be qualitatively different for different alloy systems.

Thus, in the present paper a qualitative investigation of the variations of the rolling and recrystallization textures in Cu-5%Ag alloy was carried out by determining pole figures. For the rolling and annealing textures two kinds of sample were used. The first was used to study the rolling and annealing texture development of a supersaturated solid solution which was annealed at  $900^{\circ}\text{C}$  for 7 hours, followed by water quenching. Also in order to study the effect of annealing temperature to the recrystallization textures one of the solid solution sample was annealed at  $550^{\circ}\text{C}$  and the other was annealed at  $600^{\circ}\text{C}$ . The second was designed to investigate the rolling and annealing texture development of the two phase material ( $\alpha$  solid solution +  $\beta$  solid solution) and accomplished by annealing at  $600^{\circ}\text{C}$  for three hours and then cooled by water quenching

## CHAPTER 2

### REVIEW OF PREVIOUS STUDIES

Quantative methods for pole figure measurement have been widely studied during the past thirty years. In this review an attempt is made to summarize the basic of this studies under the same heading.

#### 2.1 Rolling Textures of FCC Metals and Alloys

There are two types of rolling textures. One is expressed as copper type texture and the other is the brass type texture . The copper type texture occurs in metals of high stacking fault energy and high deformation temperatures, while the brass type texture exists in metals of low stacking fault energy at low deformations.

Textures in rolled sheet can be usually described by a fe ideal orientations in terms of the plane (hkl) that lies parallel to the plane of the sheet and the direction [uvw] that is parallel to the rolling direction. Some

typical ideal orientations are shown in Figure 1. The copper type rolling texture can be expressed as  $\{112\}\langle111\rangle$ ,  $\{123\}\langle634\rangle$ , and  $\{011\}\langle211\rangle$  components while the brass type texture is characterized by  $\{110\}\langle112\rangle$  plus  $\{110\}\langle001\rangle$  component.

A number of parameters have been suggested to characterize the fcc rolling texture transition, Figure 2. A transition from the copper type to the brass type texure which occurs on alloying has been found with decreasing deformation temperature and decreasing stacking fault energy. In case of copper alloys (2) this transition can be inferred by decreasing the temperature of rolling or by increasing of the solute content (i.e, Zn) at constant rolling temperature, as shown in Figure 3. An increasing tendency for mechanical twinning during deformation is the mechanism which causes the fcc rolling texture transition with decreasing



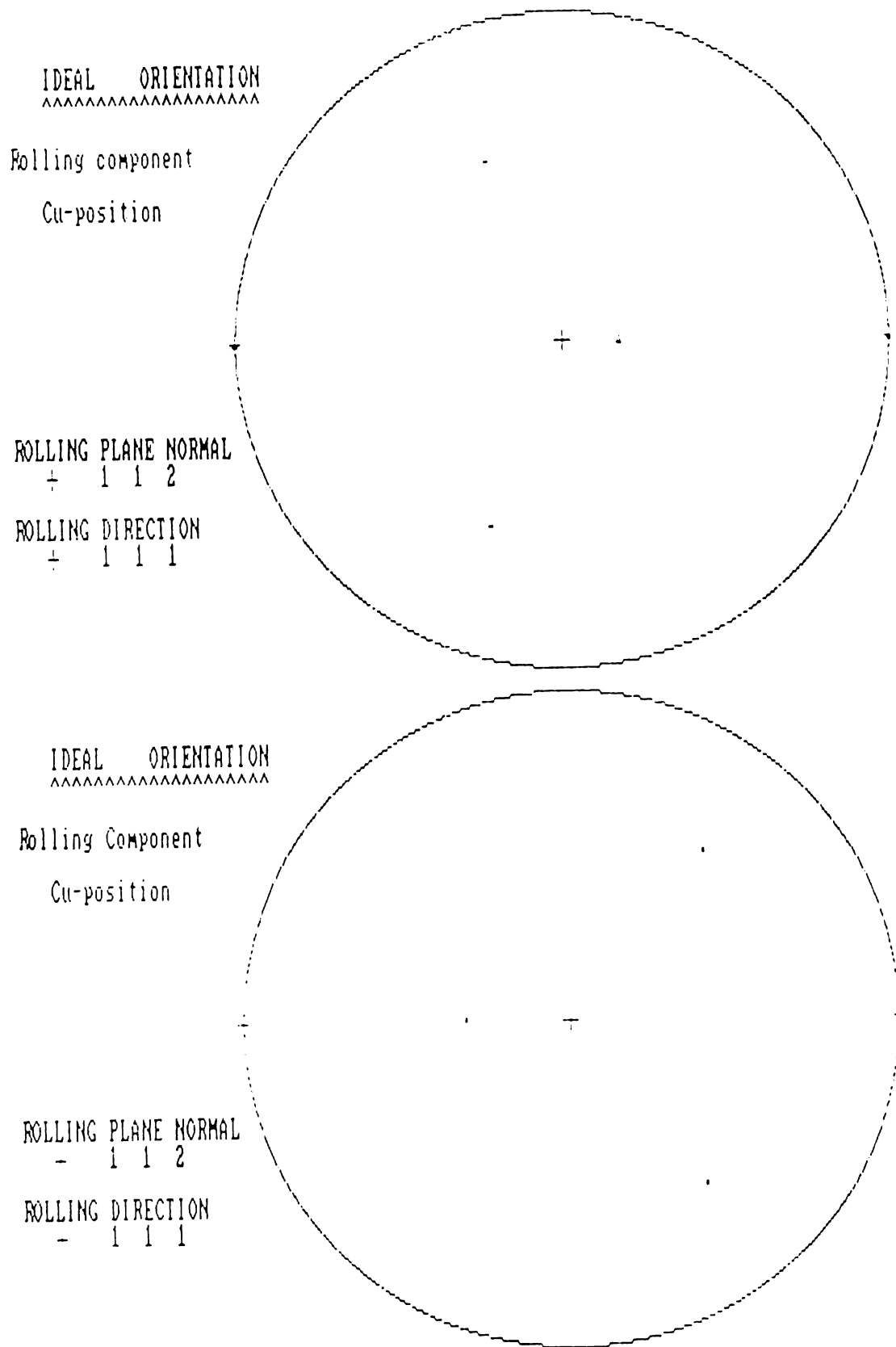


Figure 1-1. Positions of the  $\langle 111 \rangle$ ,  $\langle 200 \rangle$  poles of Cu- component of the texture





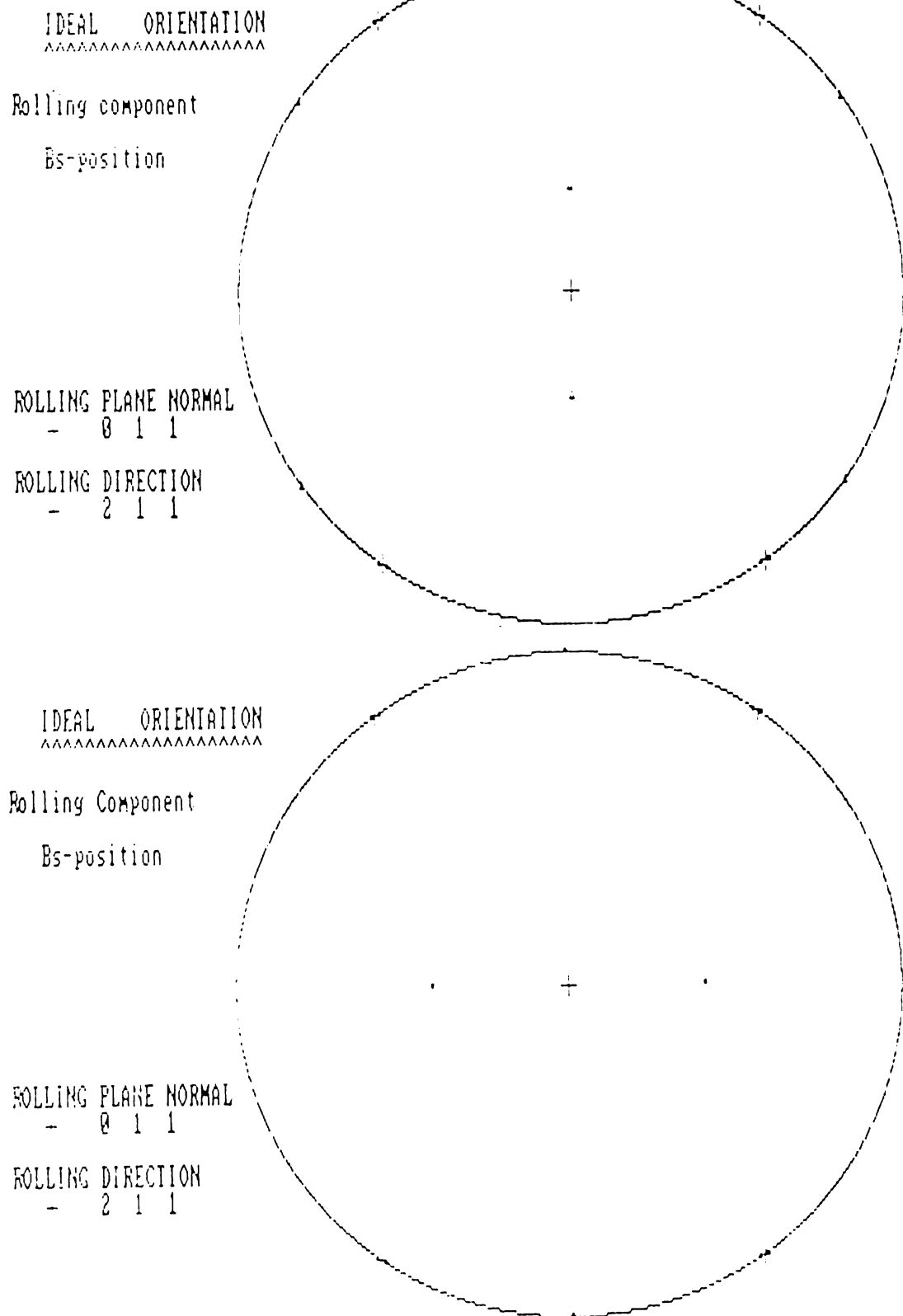


Figure 1-2: Positions of the  $\langle 111 \rangle$ ,  $\langle 200 \rangle$  poles of Bs-component of the texture

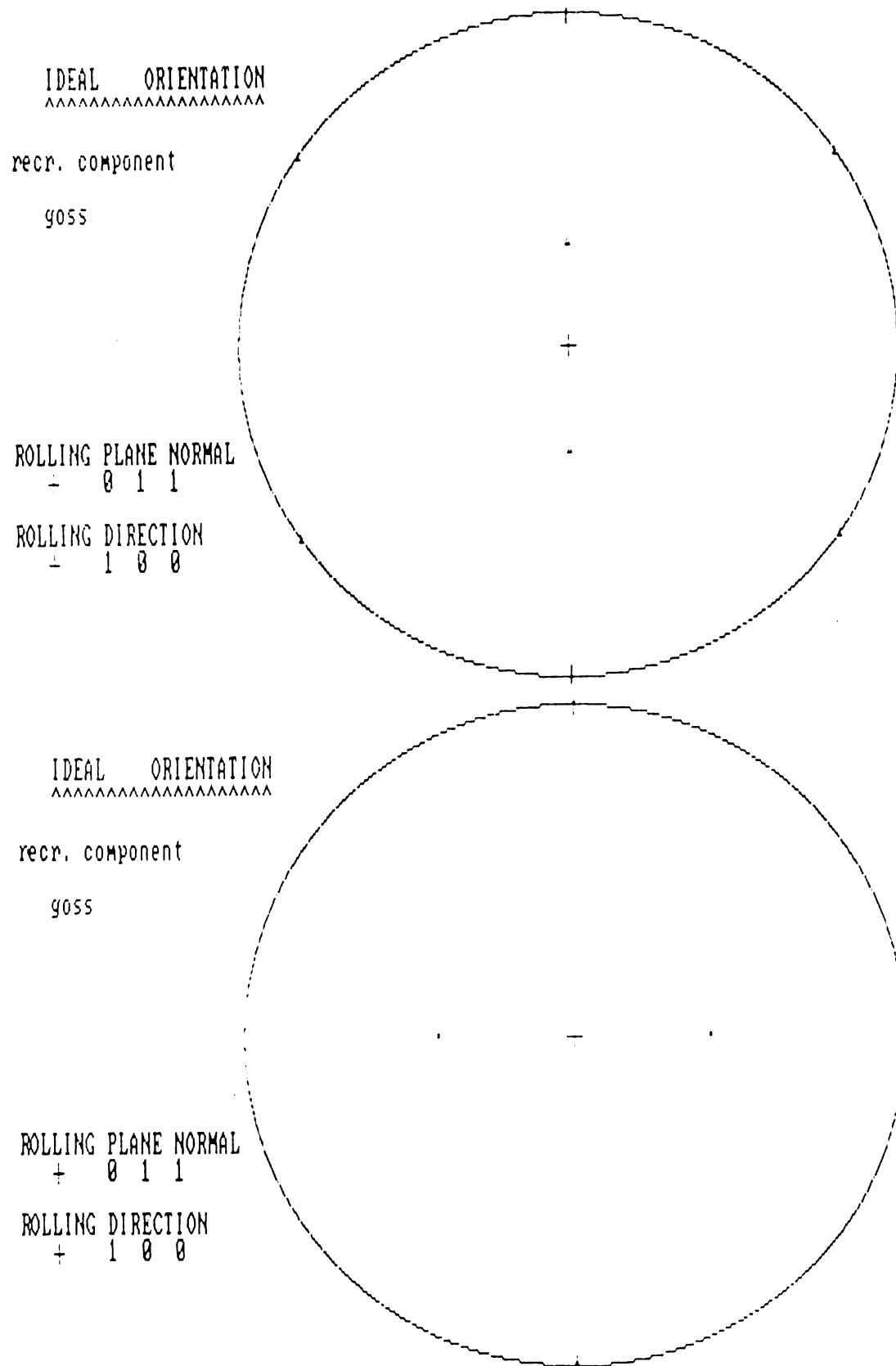


Figure 1-3: positions of the  $\langle 111 \rangle$ ,  $\langle 200 \rangle$  poles of goss- component of the texture.



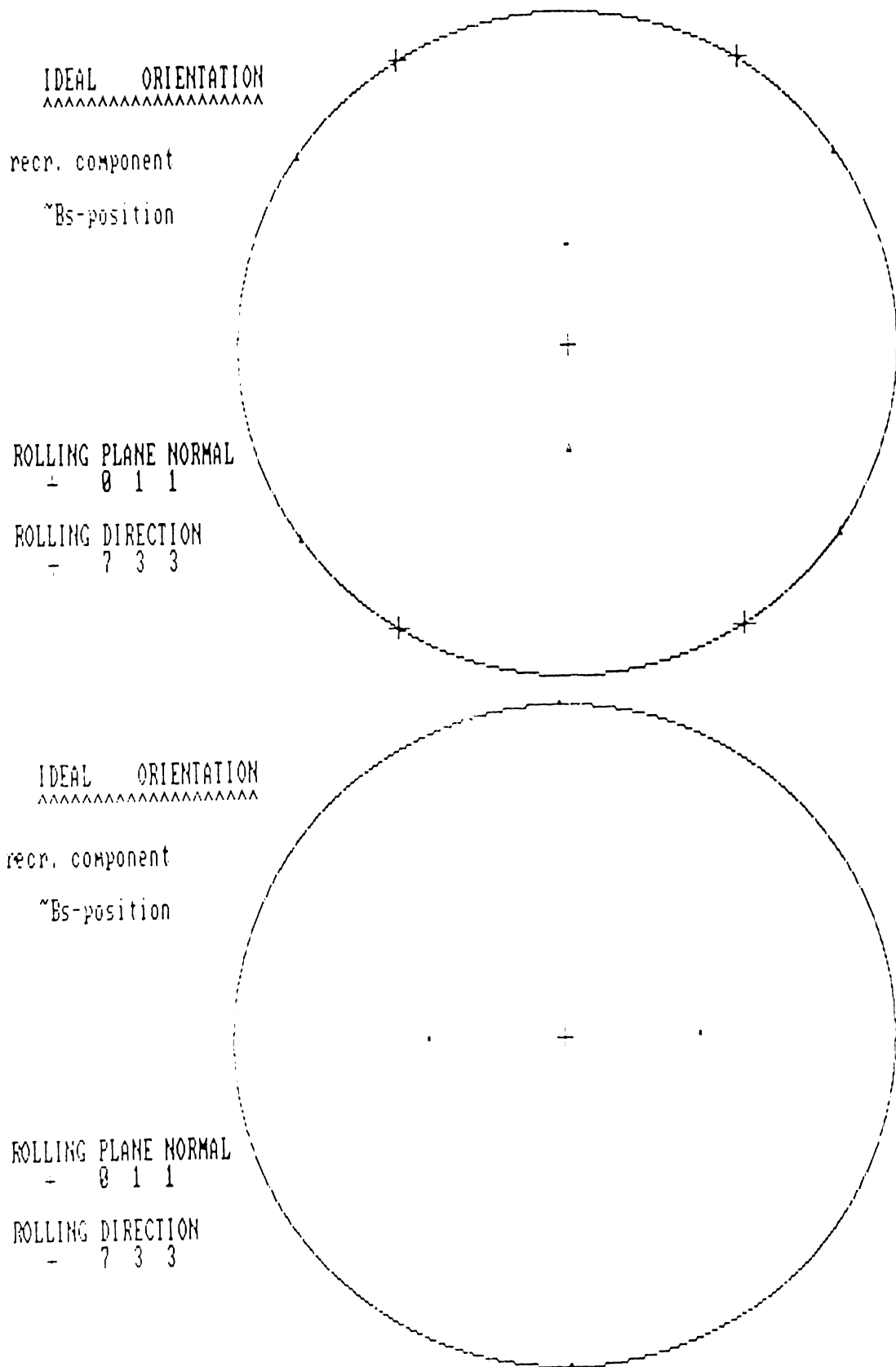
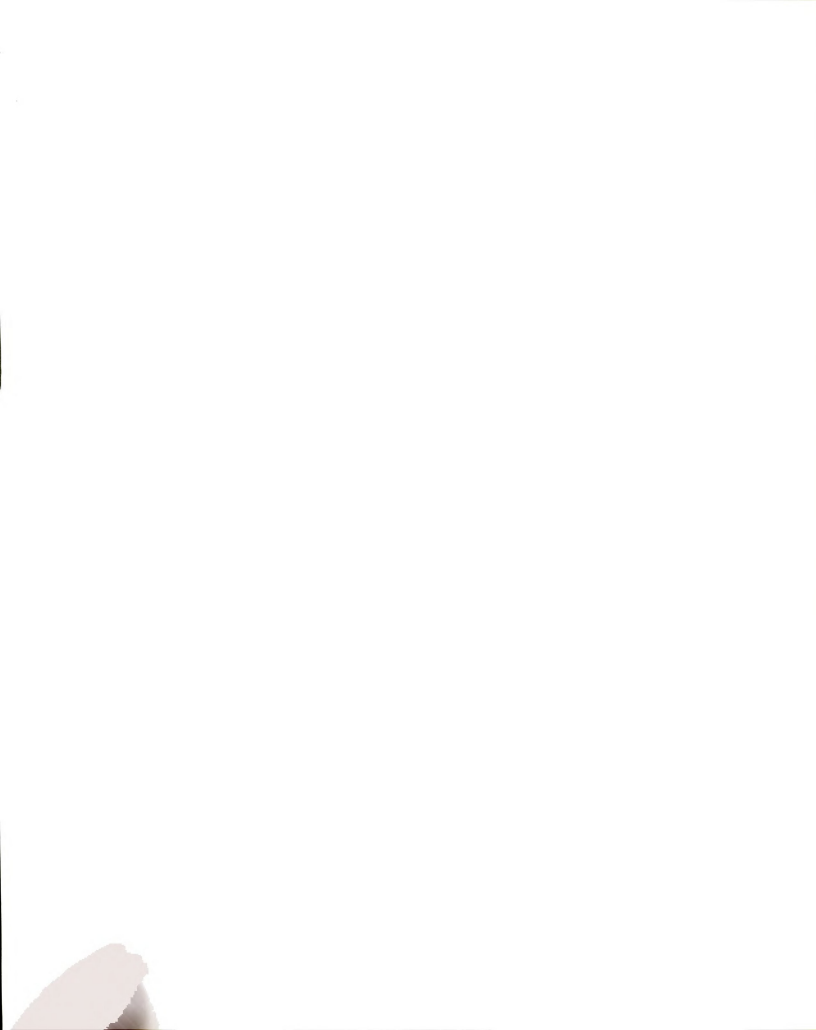


Figure 1-4 positions of the  $\langle 111 \rangle$ ,  $\langle 200 \rangle$  poles of  $\gamma$ -Bs-component of the texture



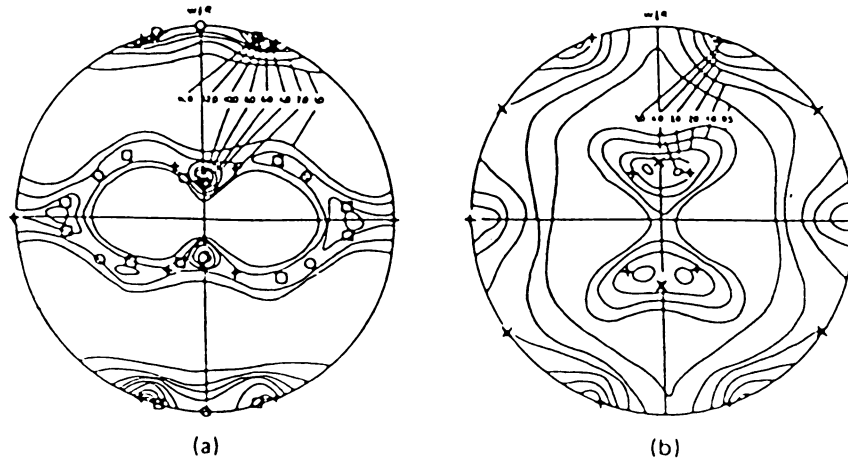


Figure 2: (111) pole figures for Cu and  $\alpha$ -brass after rolling at room temperature.

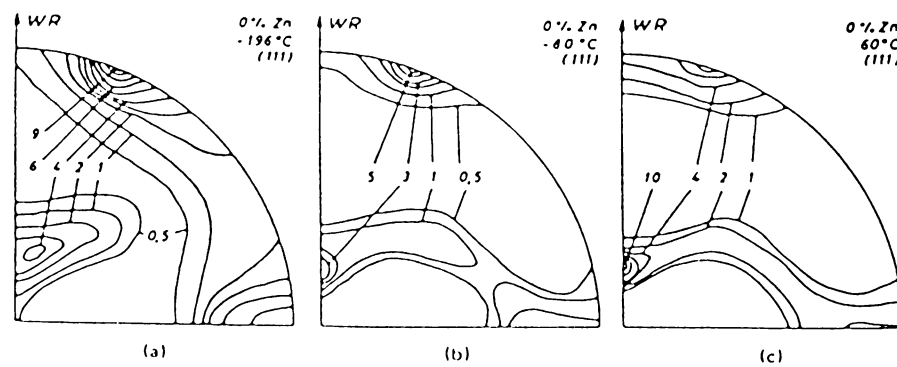


Figure 3: (111) pole figures obtained for Cu after rolling at different temperatures.

stacking fault energy,(3). Thus the copper-brass texture transition is mainly attributed to the formation of deformation twin.

## 2.2 Theories of Rolling Texture Transition

The rolling texture is formed in the course of shear deformation under the action of oriented external forces. The condition of deformation, the operative slip systems, and the behaviour of dislocations in the given material have a pronounced effect on deformation textures. The deformation structure of heavily rolled fcc materials is characterized by elongated subgrains.

Theoretical treatments of rolling texture development are based on the Sachs or the Taylor principle. The Sachs model assumes that every grain of a polycrystal has the same stress state as the macroscopically applied one. This theory failed to predict the homogeneous deformation. Thus Taylor tried a different theory which avoids this discrepancy by assuming that the strain is the same for all grains.

The rolling texture theories assume that the orientations which satisfy both the requirements of a tensile stress parallel to the rolling direction and compressive stress parallel to the sheet normal will constitute the rolling texture. The brass component of the brass type is obtained by the application of Sachs' model to the  $(111)\langle 110 \rangle$  slip deformation.

However, the Taylor theory is more adequate than Sachs's theory in predicting the constrained deformation of the polycrystalline material,(4). The calculated texture on the basis of the Taylor theory corresponds well to the experimental texture except the obvious deviation in the region of the rolling direction. Thus Honeff and Mecking (5) modified the Taylor theory by introducing the concept of partly constrained deformation of the crystallites. Figure 4(a) shows the shape of an initial cube after about 75% thickness reduction if Taylor's restriction on material flow have been obeyed. Figure 4(b) to 4(d) display schematically respective shapes if one of the three shear components have been freely chosen. Some results of partly





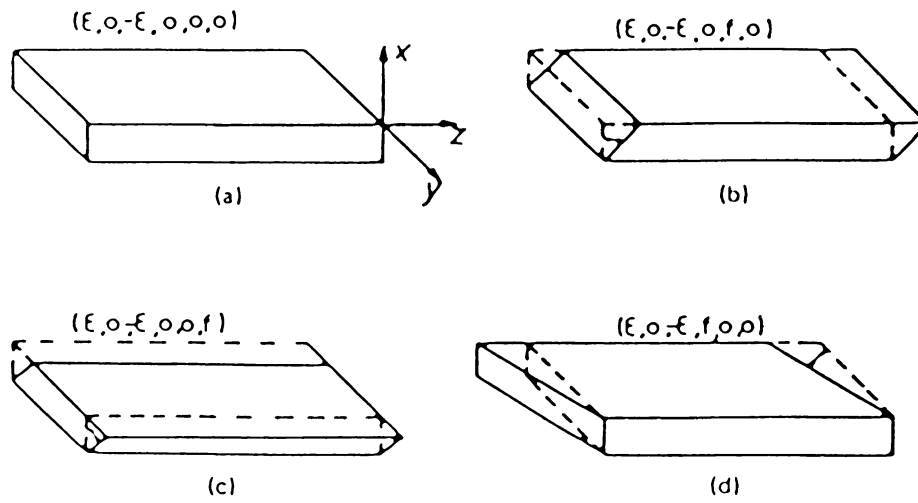


Figure 4: Shear misfit produced by the three different shear components

(a) Taylor case, (b) misfit in  $\epsilon_{xz}$ , (c) misfit in  $\epsilon_{xy}$ , and (d) misfit

in  $\epsilon_{yz}$

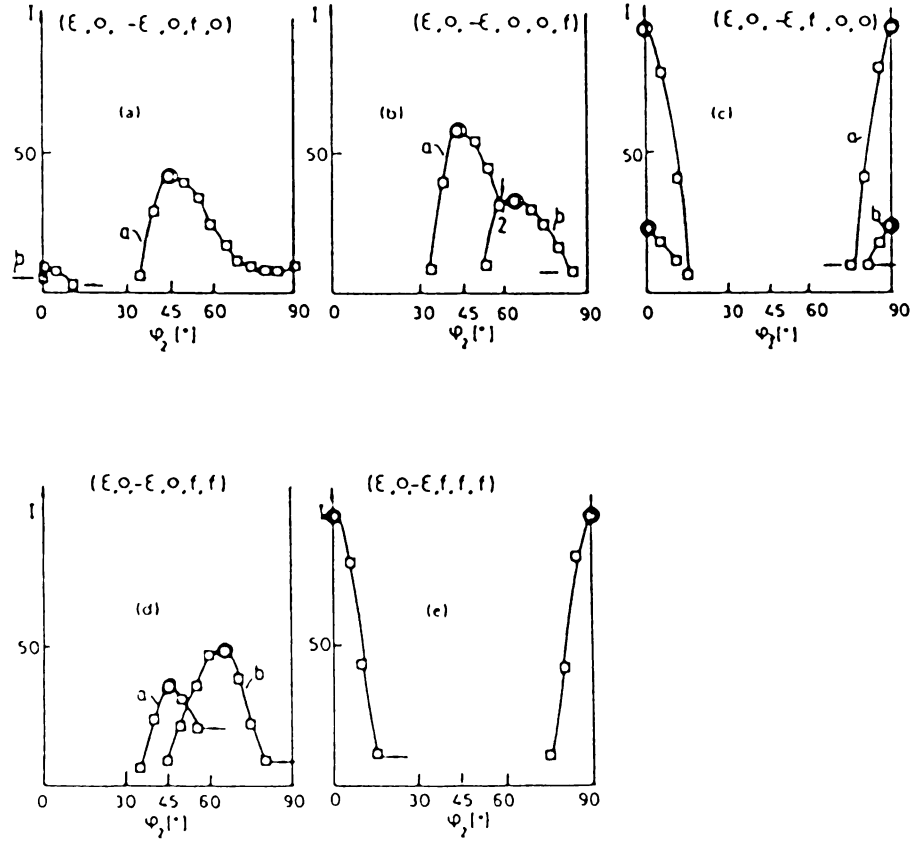


Figure 5: Orientation distribution along the skeleton line as calculated

for  $\{111\} \langle 110 \rangle$  slip according to the theory of relaxed

constraints if (a)  $\epsilon_{xz}$  (b)  $\epsilon_{xy}$  (c)  $\epsilon_{yz}$  (d)  $\epsilon_{xz}$  and  $\epsilon_{xy}$  (e) all shear

strains are assumed to be unconstrained.



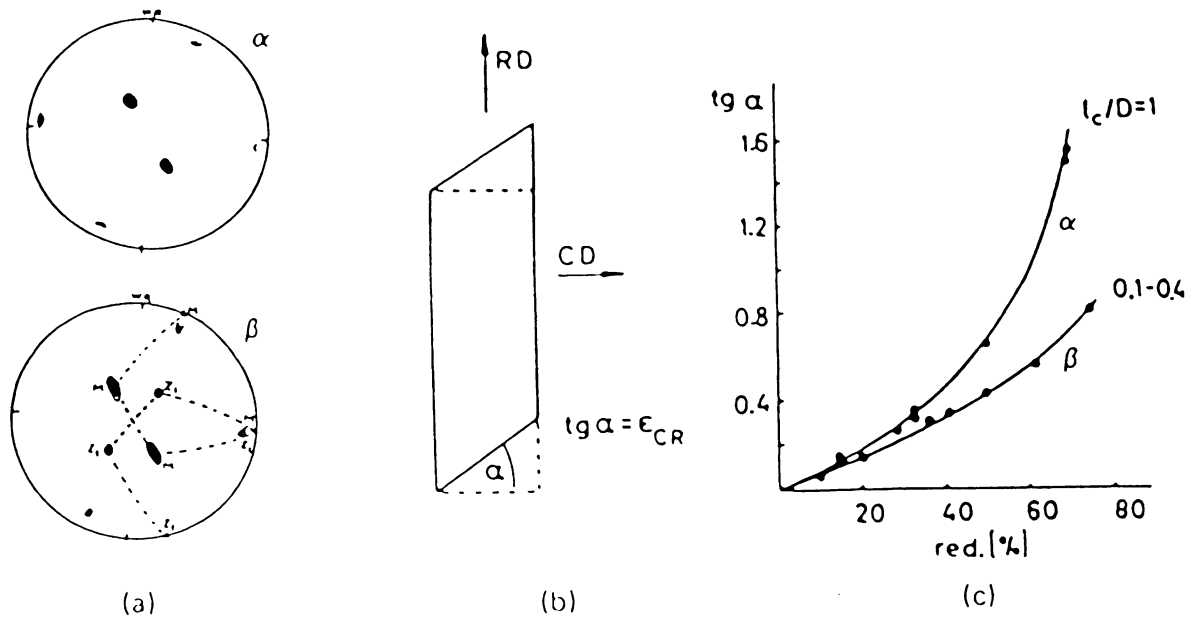


Figure 6: (a) (111) pole figures of a  $\alpha$ -brass single crystal after unconstrained rolling ( $\alpha$ ) and after rolling with constraints on  $\epsilon_{yz}$  ( $\beta$ ), which leads to twinning on the (111) plane perpendicular to RD (b) Schematic of the shape change of the initially rectangular rolling plane of the crystal. (c)  $\text{tg } \alpha$  as a function of the thickness reduction for the cases of unconstrained ( $\alpha$ ) and constrained ( $\beta$ ) deformation

constrained deformation are shown in Figure 5. The experimentally observed distribution of orientations near  $\{112\} \langle 111 \rangle$  and  $\{123\} \langle 634 \rangle$  in figure 4(d) can be explained by the theory of the relaxed constraints for flat grains where the shear misfit in  $\epsilon_{xy}$  and  $\epsilon_{xz}$  is considered to be unimportant. The brass component is due to the unconstraints of  $\epsilon_{yz}$  rather than unconstraints of  $\epsilon_{xy}$  and  $\epsilon_{xz}$ . However  $\epsilon_{yz}$  is not characteristic of the flat grains since there the constraints on  $\epsilon_{yz}$  are very strong.

Thus the development of brass texture has to be explained in a different way, which is possible by taking into account the effect of the anisotropy of the environment of the grains, (4). This aspect is to be considered in textured materials and attains particular importance in the context of twinning, since twinning leads to fixed orientation relationship between neighboring crystallites.

How twinning influences the constraints is shown well in the brass single crystal experiments (6). After rolling brass single crystal with  $\{110\} \langle 112 \rangle$  orientation, this remains stable. Thus a shear component  $\epsilon_{yz}$  which converts the rectangular rolling plane into a parallelogram is developed. If the same crystal is rolled with constraints on  $\epsilon_{yz}$ , twinning occurs on  $(111)$  plane perpendicular to TD. Thus the single crystal is split into alternating lamellae of twins and matrix, which have the two crystallographically equivalent orientations  $(110) [-112]$  and  $(\bar{1}\bar{1}0) [112]$ . These components produce shear strains  $\epsilon_{yz}$  that are opposite in sign and thus cancel each other on the macroscopic scale, so that the internal reaction stresses are drastically reduced. Therefore the crystallites of the two complementary  $\{110\} \langle 112 \rangle$  orientations slip like unconstrained single crystal.

### 2.3 Annealing Textures of FCC Metals and Alloys

If a deformed material with a deformation texture is annealed, a recrystallization texture



occures in it, which can be either identical to or different from the deformation texture.

Figure 7 shows typical texture after rolling and subsequent primary recrystallization in f.c.c. metals. The rolling texture of copper produces the cube texture (a and b), the brass rolling texture forms the brass recrystallization texture which has  $\{326\}\langle 835 \rangle$  as the main component (e and f). An intermediate rolling texture transforms into an intermediate recrystallization texture, (c and d).

Since a recrystallization texture is determined by the structure formed during deformation, nucleation from the deformed state is of primary interest in recrystallization textures. Many possible nucleation mechanisms have been suggested. The most significant nucleation mechanisms (7) are summarized in the following.

1. Nucleation at preexisting grain boundaries by strain induced grain boundary motion on moderately deformed materials.
2. Preferred nucleation in regions of strong orientation gradients in heavily deformed materials.
3. Nucleation by subgrain growth in a homogeneous deformation structure.

However even orientations of high nucleation rate may not exist in the recrystallization texture in practice. Thus the theory of oriented growth was proposed by Beck (8). According to this theory nuclei with diverse orientations exist in the early stage of primary recrystallization, but then only the nuclei whose orientation relative to the textured deformed matrix provides to the highest mobility of their boundaries will succeed during. In fcc metals grain boundaries with an orientation related to the matrix by rotations  $40^\circ \langle 111 \rangle$  have been found as high growth rate boundaries (9). While the orientation of recrystallization nuclei repeats the orientation of the deformed matrix the growth rate is the result of the competing

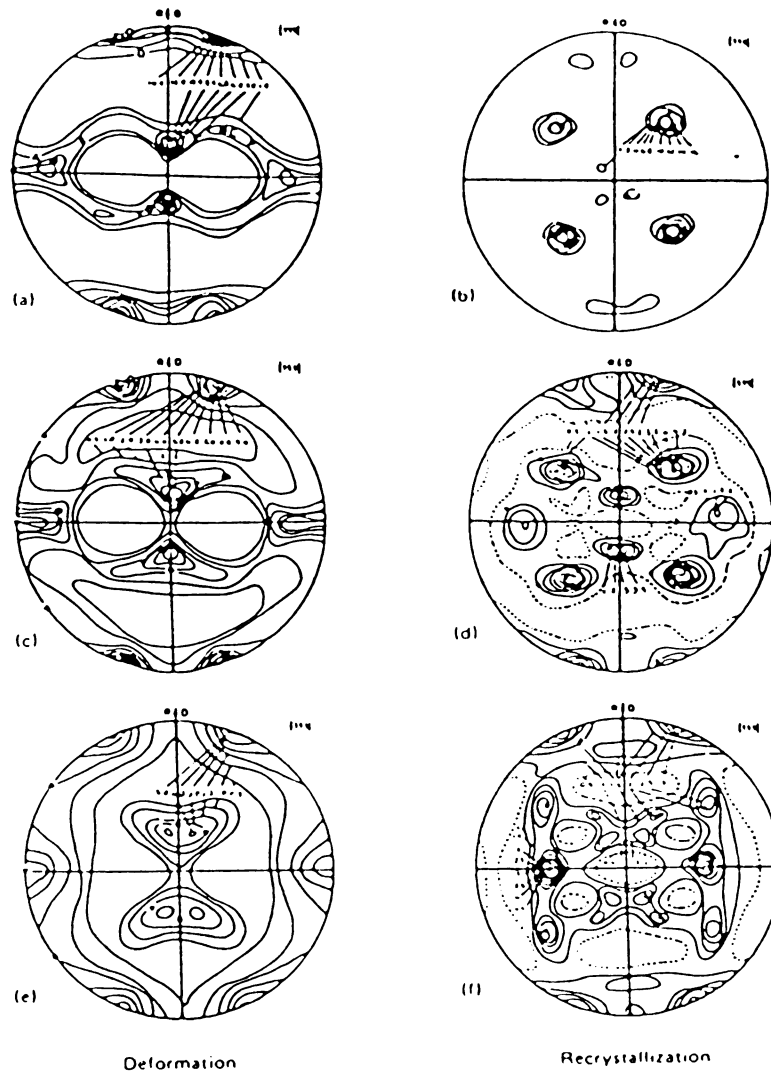


Figure 7 : (111) pole figures of rolling textures of Cu-Zn alloys before and after recrystallization. (a),(c),and (e) subsequent to rolling with 95% thickness reduction of (a)Cu and(c)Cu-5%Zn at room temperature and (e) Cu-5% Zn at 77°K. (b),(d), and (f) show the corresponding textures after primary recrystallization.





effect of the driving and retarding forces, which is determined by the interaction of numerous factors. One or another of these factors decide which of the two processes, either nucleation or grain growth is predominant. Thus the development of recrystallization textures can be regarded as a combination of these two theories.

#### 2.4 Theories of the Development of Recrystallization Texture.

An fcc metal with a low stacking fault energy, if rolled at a low energy temperature, develops a texture with a strong  $\{110\}\langle 112\rangle$  component and a somewhat weaker component in  $\{110\}\langle 001\rangle$  as in Figure 7. The corresponding texture after primary recrystallization again shows maxima of intensity in two positions, namely, rather high intensity in  $\{326\}\langle 835\rangle$  and slightly less in  $\{013\}\langle 100\rangle$ , as seen in Fig 7f.

In Figure 8 the precise positions of the  $\langle 111\rangle$  poles of the two complementary  $\{110\}\langle 112\rangle$  (I and II) components are shown (10). I and II are twin related and thus have the peculiar property that from the eight orientations obtained by  $40^\circ$  rotations around the  $\langle 111\rangle$  poles of one component, each orientation happens to become a neighbor of one of the eight orientations produced by the  $40^\circ$  rotations of the other component. Because of the orthorhombic symmetry of the rolling process, the eight possible orientation pairs consist of only three crystallographically different sets. One of each set of orientation pairs is given in Fig. 8b-d. It is a striking fact that the recrystallization components  $\{326\}\langle 835\rangle$  (b),  $\{013\}\langle 100\rangle$  (c), and  $\{211\}\langle 011\rangle$  (d) represent fast-growing orientations with respect to both  $\{110\}\langle 112\rangle$  components of the rolling texture.  $\{211\}\langle 011\rangle$  (d) has never been observed in recrystallization textures while  $\{326\}\langle 835\rangle$  (b)  $\{013\}\langle 100\rangle$  are observed frequently. Thus there should be some other selection principles. It seems to be related to the nucleation mechanisms.

However there are some observations which do not fit into the concept of the compromise orientations based on  $40^\circ$  rotations. For the Cu-p alloys (10) different orientation

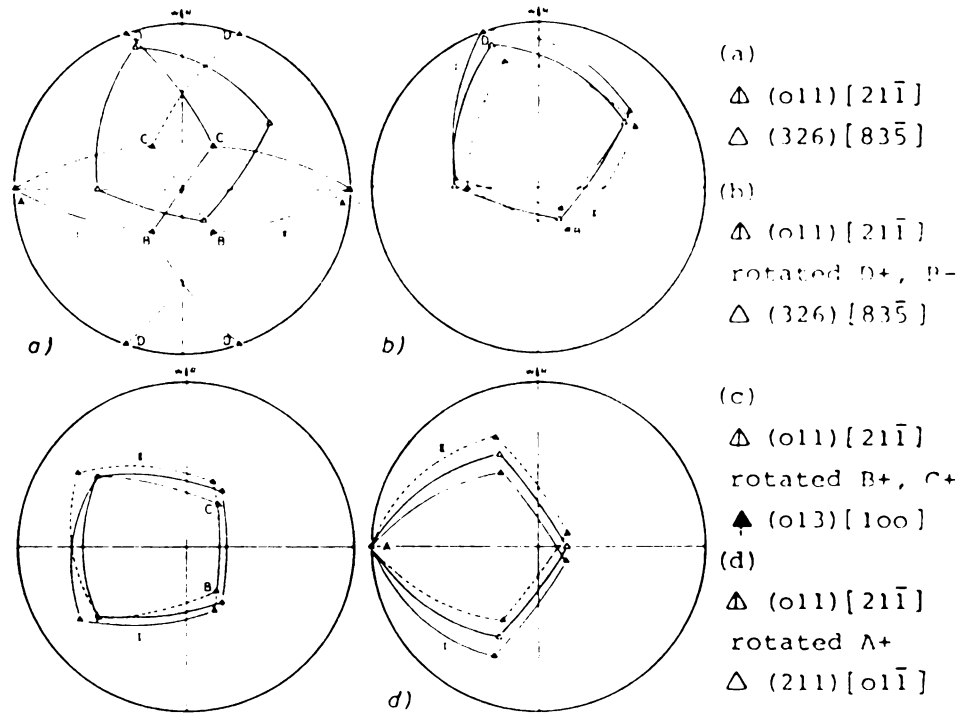


Figure 8 :  $40^\circ \langle 111 \rangle$  rotations of both components of the (011)[21 $\bar{1}$ ] orientation.

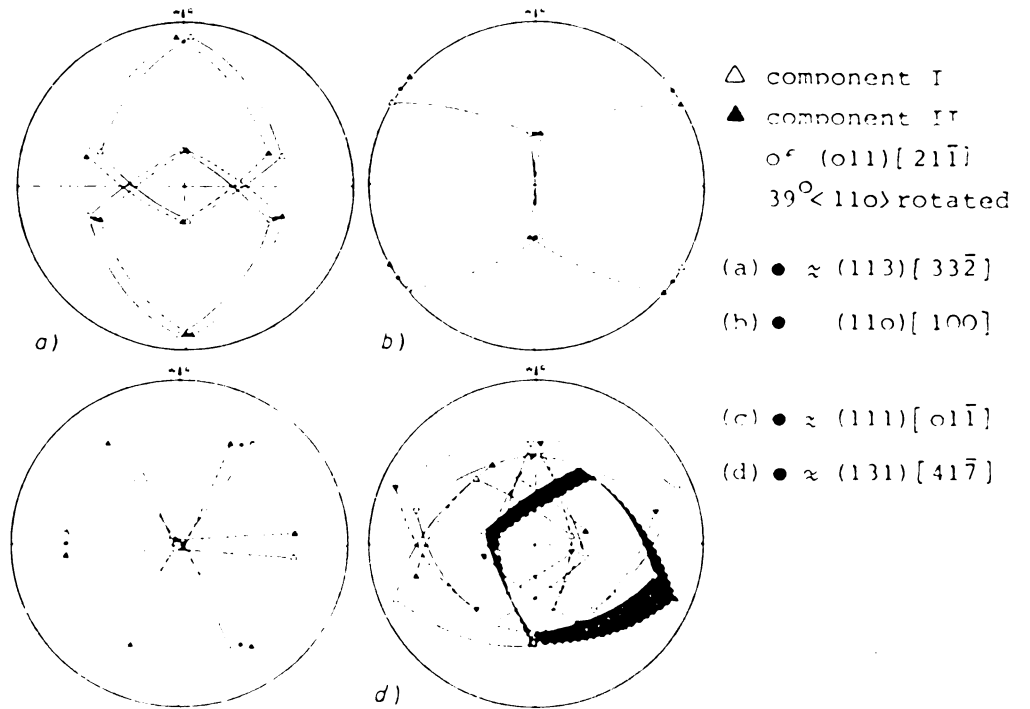


Figure 9 :  $39^\circ \langle 110 \rangle$  rotations of both components of the (011)[21 $\bar{1}$ ] orientation

relationship between deformation texture and recrystallization texture was found not  $40^\circ \langle 111 \rangle$  rotations but  $38.9^\circ \langle 110 \rangle$  rotations shows the highest growth rate. Upon these rotations four compromise orientations are found with respect to the  $(011) \langle 211 \rangle$  orientation as illustrated in Figure 9. The two compromise orientations,  $(113) \langle 332 \rangle$  and  $(011) \langle 100 \rangle$  are observed in practice.

Base on these findings it can be concluded that selected growth is the dominant mechanism for recrystallization texture development in low stacking fault energy materials.

## CHAPTER 3

### EXPERIMENTAL PROCEDURE AND TECHNIQUES

#### 3.1 Pole Figure System

The orientation distribution of crystallites in polycrystalline materials, i.e. textures, have been investigated mainly by X-ray texture goniometers. In the following how the goniometer scan a whole pole figure projection will be discussed.

##### 3.1.1 Principles of X-ray Texture Goniometers

The crystallographic orientation  $g$  of an individual crystallite in a polycrystalline sample is defined by the orientation of its crystal coordinate system  $K_C$  with respect to the sample coordinate system  $K_S$ . The orientation  $g$  of  $K_C$  with respect to  $K_S$  can be described by the angles  $\alpha$ ,  $\beta$  of a direction  $[uvw]$  and the rotation angle  $\gamma$   $[uvw]$ . If the direction  $[uvw]$  is the normal to the reflecting lattice plane  $(hkl)$  then the reflected intensity is independent of a rotation of the crystal through angle  $\gamma$ . Thus polycrystal diffraction yield the orientation distribution of the crystal direction  $[uvw]$  as a function of  $\alpha$  and  $\beta$ . This is called as  $(hkl)$  pole figure(11).

In order to measure the pole figure it is necessary to rotate the sample through three angles is provided. This enables one to bring a sample fixed coordinate system  $K_S$  into any position with respect to a laboratory system  $K_L$ . In the start position  $K_S$  is parallel to the  $K_L$ . Then the sample is rotated successively

1 about  $X_S$  through  $\varphi_1$



2. about  $Y_s$  through  $\phi$

3. about  $X_s$  through  $\varphi_2$

In the back reflection technique (12) a sheet sample is mounted on the sample holder with its normal direction parallel to the axis of the  $\varphi_2$  rotation. This leaves the choice of setting the rolling direction parallel to  $Y_s$  or  $Z_s$ . If we set it as  $Y_s$  the sheet has the orientation.

$$Y_s // RD, Z_s // TD, X_s // ND \quad (1)$$

in the sample holder as shown in Figure 10. Then the sheet is set at the angles  $\varphi = \theta_{hkl}$ . This is shown in Figure 11. With  $\phi$  and  $\varphi_2$  in the zero position the diffraction vector  $d$  which bisects the angle between incident and reflected beam is parallel to  $Z_s$ . By the rotation  $\phi$  and  $\varphi_2$  the diffraction vector is brought into the position  $(\alpha, \beta)$  as shown in Figure 12. Where  $\alpha$  and  $\beta$  are the pole figure angle defined with respect to its sheet coordinate system RD, TD, ND as shown in Figure 11. Thus this motion is characterized by

$$\varphi_1 = \theta = \text{const.} \quad (2)$$

and the pole figure angles are related to  $\phi$  and  $\varphi_2$

$$\alpha = 90 - \phi \quad \beta = 90 + \varphi_2 \quad (3)$$

where  $\phi$  and  $\varphi_2$  are taken positive in the sense of a right handed screw about the  $Y_s$  and  $X_s$  directions respectively.

### 3.1.2 Pole Figure Projections

Most pole figures in the metallurgical literature are projected in the stereographic projection. Because this projection is angle true and measurement of angle is simplified.

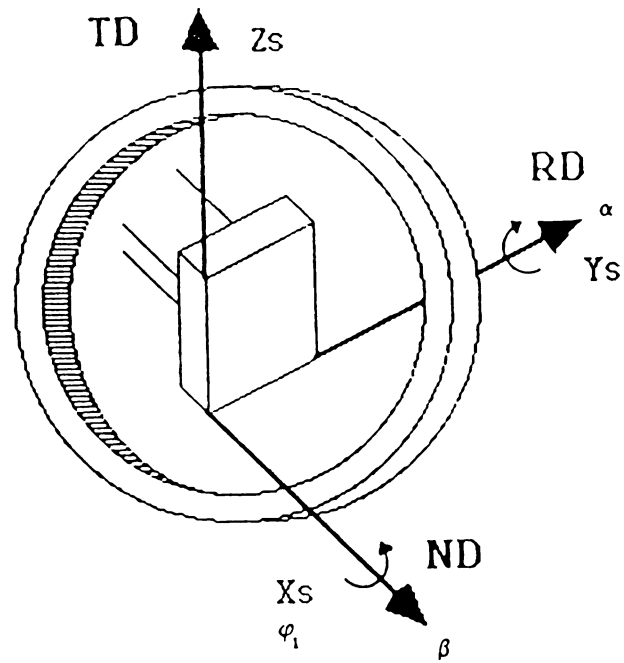


Figure 10 : A sheet sample mounted in back-reflection position.

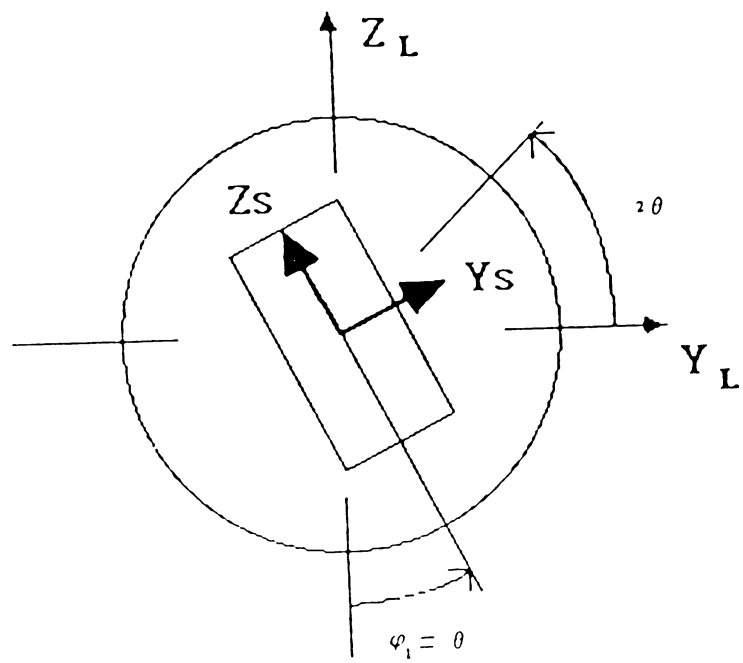


Figure 11 : Starting position of the sample





Simultaneous rotations in the  $\alpha$  and  $\beta$  modes, when the pole figure device is measuring in reflection, cause the normal to the reflecting planes to describe a spiral in the plane of stereographic projection, Figure 13. The intensity of a pole along the spiral is plotted on the projection. Figure 14 is the illustration of this principle. The normal CP is represented by its pole p, which is the intersection to p with the reference sphere. The pole p is represented by its stereographic projection p'. This geometry is drawn in two dimensions as shown in Figure 15. With this one can derive the radius for a certain position on the pole figure projection.

$$R' = R \sin \alpha / 2 \quad (4)$$

If  $\alpha$  is too large the irradiated region may become larger. And for  $\alpha \neq 0$  the focussing condition is only fulfilled for the central line of the ample. These conditions reduce the reflected intensity according to  $\alpha$ . However, if the reflected intensity is being compared with the corresponding intensity from a random sample, the calculation of the correction factors can be avoided (13). The calculation of the normalization condition from definition.

$$P_{hkl}(\alpha\beta)_{\text{random}} = 1 \quad (5)$$

$$I'(\alpha\beta) = I'_{\text{random}}(\alpha) P_{hkl}(\alpha\beta) \quad (6)$$

Eq(6) gives the pole density in multiples of the random density.

### 3.2.3 Installation of Pole Figure System

A Norelco wide range goniometer was mounted on a diffractometer base. The collimator was aligned to the "spot focus" window of the X-ray tube (port No.3). In order to fulfill the geometry of scanning the following conditions were maintained during assembly procedure.

1. The distance between the center of the X-ray tube and the center of the sample should be 170mm.
2. The distance between the top surface of the sample holder and the basic unit

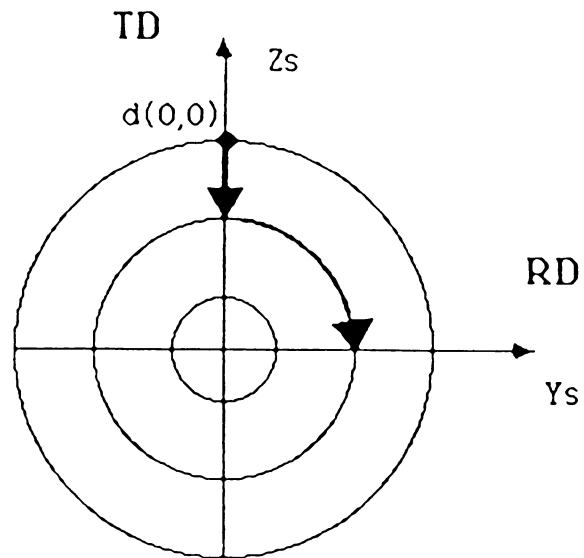


Figure 12 · The diffraction vector  $d$  is brought into the sample direction  $\{\alpha, \beta\}$  by the rotations  $\phi$  and  $\phi_1$ .

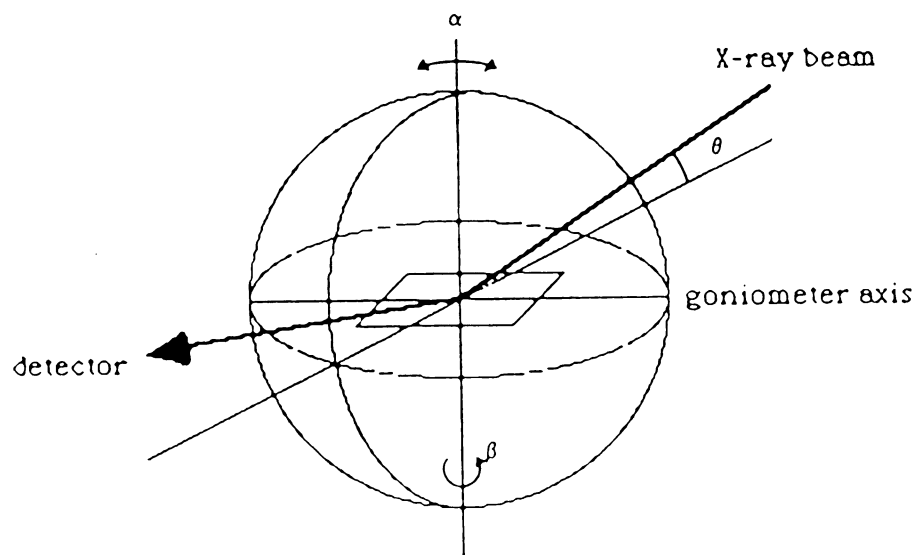


Figure 13 · Geometric illustration of axial motion

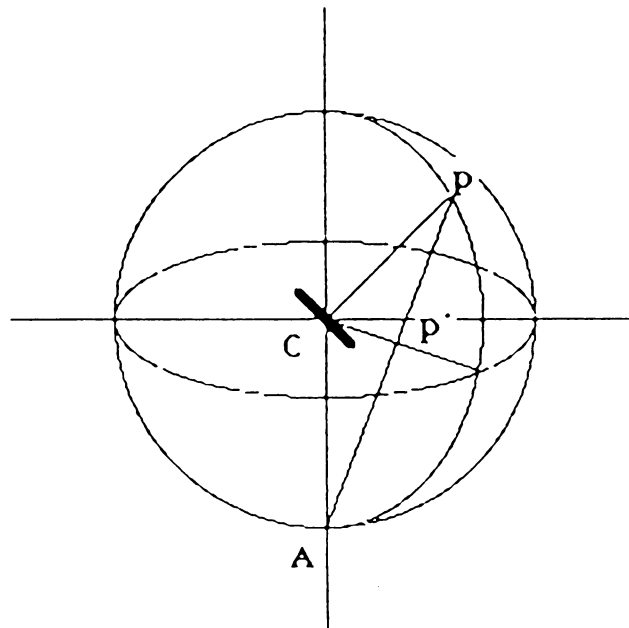


Figure 14 : The illustration of pole figure projection.

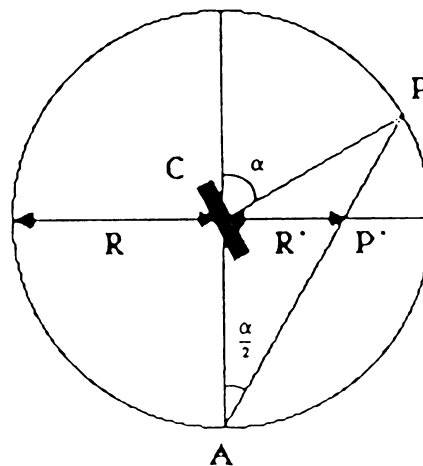


Figure 15 : The two dimensional illustration of pole figure projection

table top should be 260mm.

3. The distance between the shutter assembly and the collimator should be as short as possible without making contact.

4. An image of the exit opening of the collimator with dimensions of approximately  $4 \times 1 \text{ mm}^2$  rectangular should be visible on the fluorescent disc.

An IBM XT computer was adapted to the counter electronics through a WB-AIO-B Analog-to-digital converter for the automatic determination of pole figures. This analog card was installed in the connector slots located inside the IBM computer. The recorder output was connected to the terminal box. The software of this analog card was set up to select the voltage range as 50mv. This system configuration is shown in Figure 16.

In order to check the accuracy of this system, an aluminum single crystal and lithium fluoride single crystal was used as the test material. The orientation of the single crystals were determined by Laue patterns. The results are shown in Fig

Usually it is not possible to indicate the rolling direction in the pole figure exactly. Thus the rolling direction on the measured pole figure is not in a correct position. It is then more accurate to determine it by symmetry considerations from the pole figure measurements themselves. This is achieved by rotating the pole figure through an appropriate angle. Then the correctly adjusted symmetric pole figure is obtained.

The calculation of the correction factors (ie geometrical factor, defocusing factor, and absorption factor) can be avoided if the reflected intensity is being compared with the corresponding intensity reflected from a random sample under the same conditions.

#### 3.2.4 Software system

This system can be divided in three parts as shown in Figure 17. The first is used for data acquisition. The second is the pole figure plotting program. The third is applied to the second part

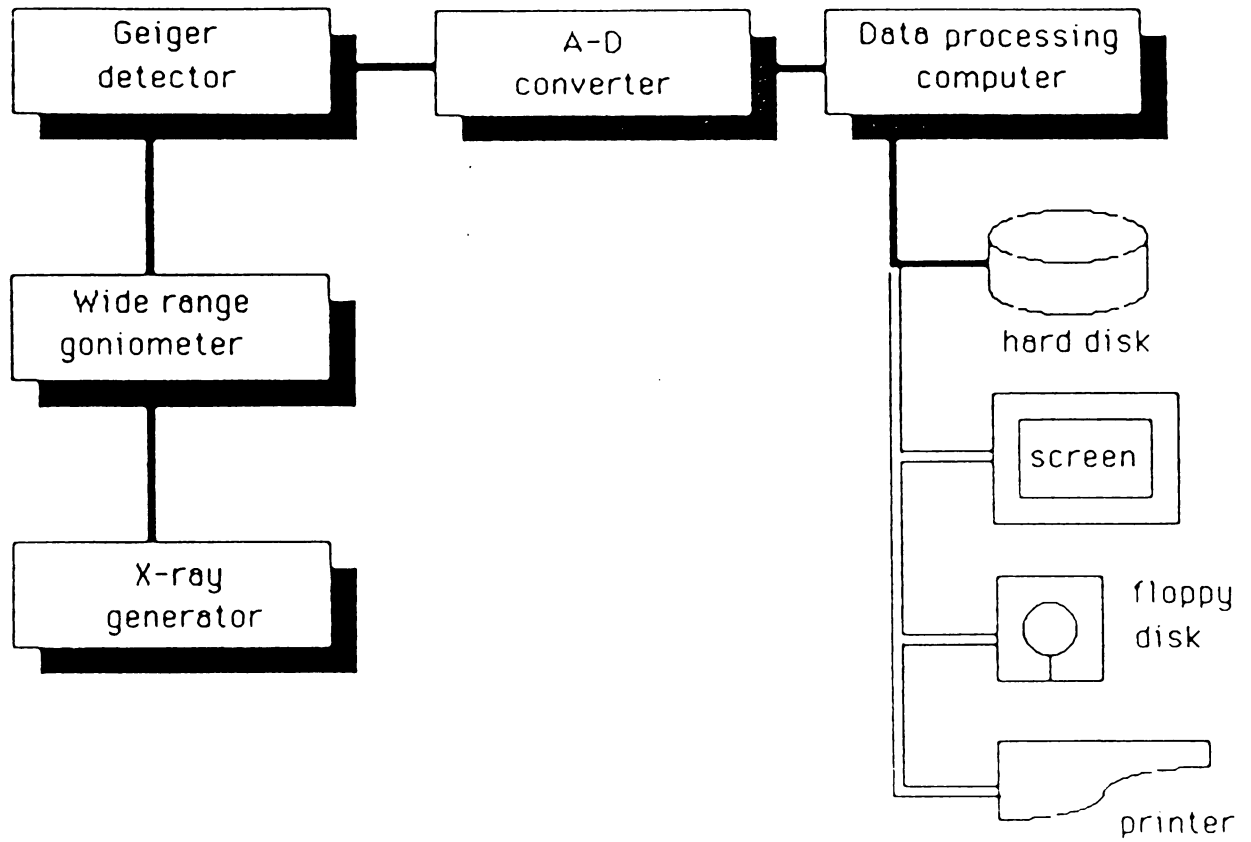
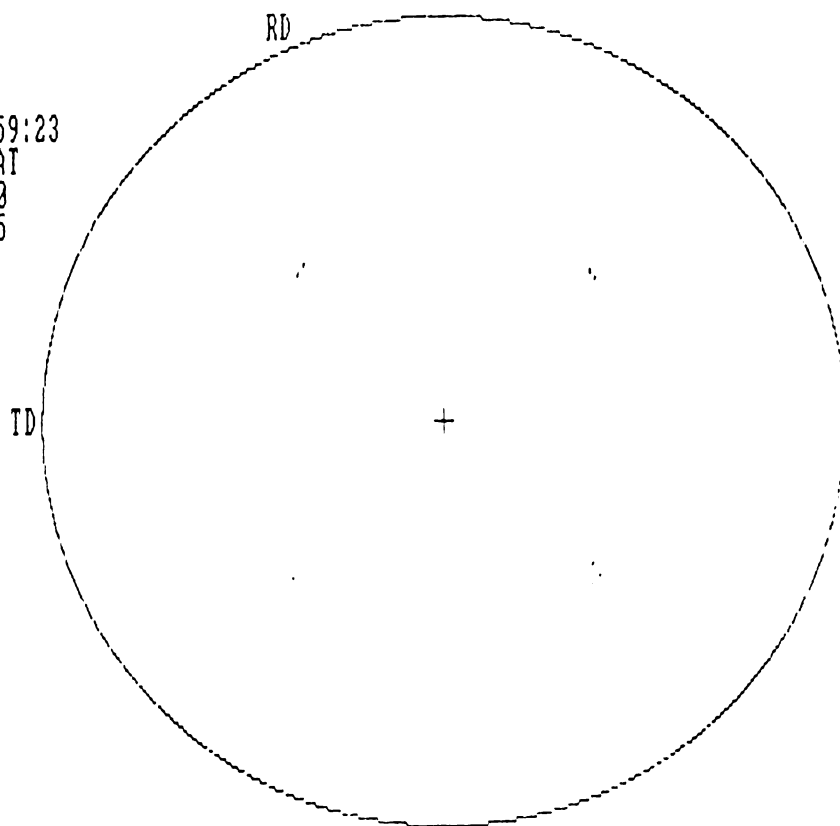


Figure 16 : Pole figure system configuration.

POLE FIGURE  
 ^^^^^^^^^^^^^^^  
 01-30-1986 00:59:23  
 FILE NAME : LIF.DAT  
 X-ray : KV 30  
 MA 15  
 H K L : 111  
 SCALE : 1  
 PITCH : 2.5  
 ROT. STEP : 2.5

DEN	VOLTAGE
0	0.000
1	4.832
2	9.665
3	14.497
4	19.329
5	24.162
6	28.994
7	33.826



POLE FIGURE  
 ^^^^^^^^^^^^^^^  
 01-30-1986 01:04:42  
 FILE NAME : ALSI1.D  
 X-ray : KV 30  
 MA 15  
 H K L : 111  
 SCALE : 1  
 PITCH : 2.5  
 ROT. STEP : 2.5

DEN	VOLTAGE
0	0.194
1	5.484
2	10.967
3	16.451
4	21.934
5	27.418
6	32.901
7	38.579

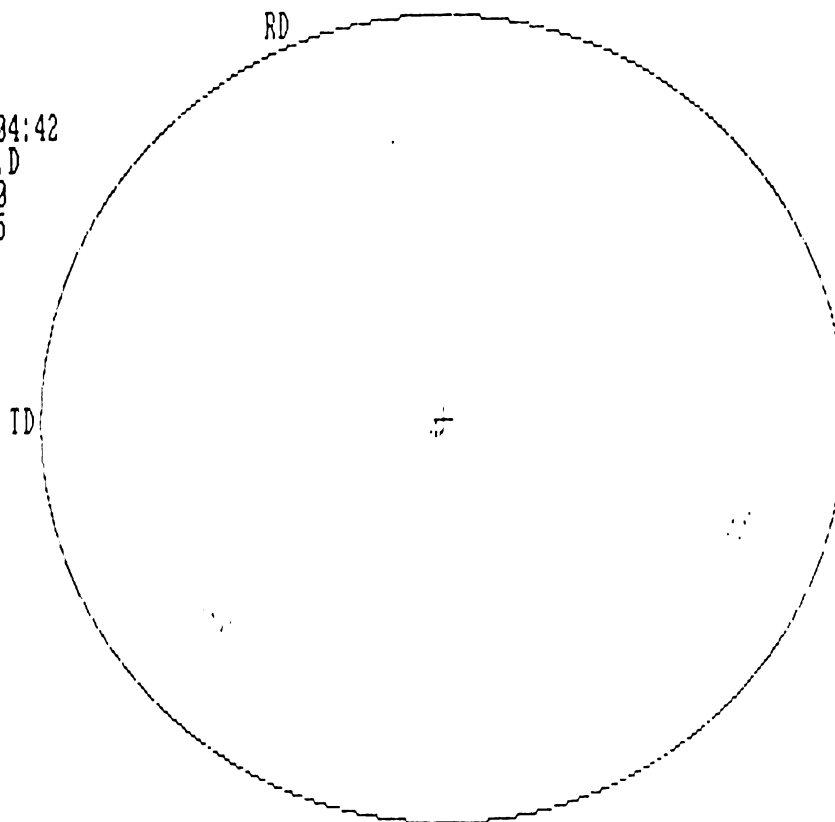


Figure 17 - (111) pole figures of a lithium fluoride single crystal and an aluminum single crystal.

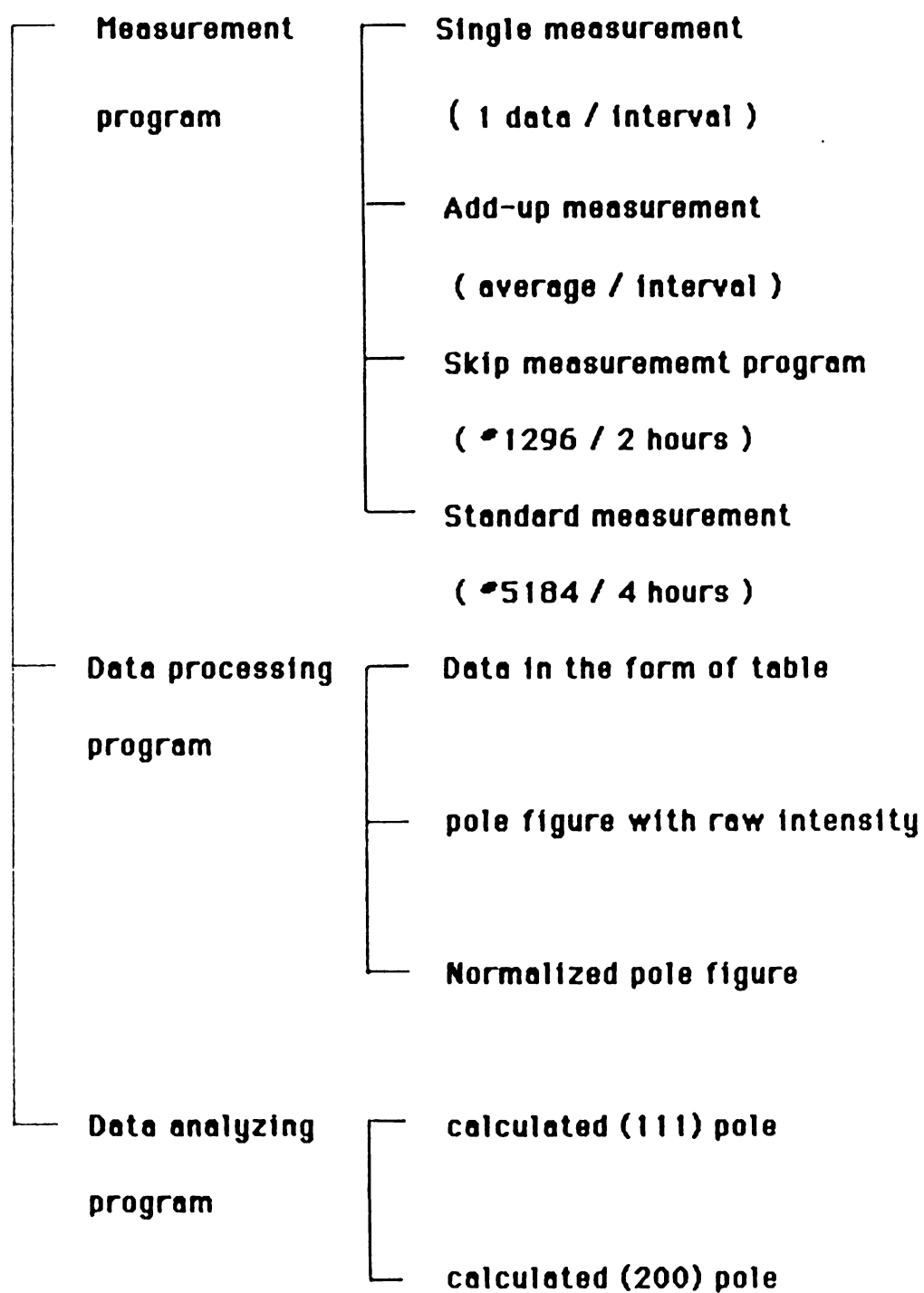


Figure 18 : Pole figure software system configuration



and this enables us to figure out components of the pole figure.

The measured intensity data from the data acquisition program are not yet pole density values. The calculation of the correction factors can be avoided if the reflected intensity is being compared with the corresponding intensity reflected from a random sample under the same condition. In order to obtain pole density corrections have to be applied which are carried out by the normalized pole figure program. This normalization was done by the large number of randomly oriented grains, i.e., a powder sample and expressed as times random. The average intensity of the powder sample is calculated in each step of  $\alpha$  motion and the measured intensity is divided by this value. The final step of measuring process is the data output or data storage. After the measurement the representation of the data is made by simulating a graphic on the printer. The graphic output is represented by special symbols, each symbol characterizing a specific pole density level, as shown in Figure 20. Sometimes we need the graphic output with only higher density poles. It allows a quick inspection of the measured pole figure. Equidensity lines can then be drawn by hand in the standard graphic output.

### 3.2.5 Operation of the System

1. The maximum dimensions for a sample are 45mm (largest diameter) and a thickness of 6mm.
2. Mount the sample on the sample holder using a suitable adhesive (A plastic clay was used as an adhesive in this work).
3. Insert the sample holder with a rolling motion.
4. Adjust the height of the sample with the adjust pin.
5. Adjust the desired rate of oscillation by setting the linkage arm in the appropriate hole in the disc.
6. Set the large degree scale ( $\alpha$ ) and the small degree scale according to the

desired program. ( The relations between switch setting and measurement program are tabulated in Table 1.)

7. Turn the  $2\theta$  crank to the desired angle. ( the angle is determined by Bragg's law and thus depends on wave length, lattice parameter of material and desired reflection plane. Calculated angles are tabuated in Table 2.)

The lattice parameters of copper silver solid solutions have been measured by Owen and Rogers ( 14) the angles were calculated based on this result.

### 3.2 Specimen Preparation

#### 3.2.1 Rolling process of Cu 5% Ag

The specimens were cut with 6x7 mm cross-section and a length of about 13mm, with no initial deformation caused by machining. In order to get a random texture the alloys were homogenized at 920°C for several hours.

The samples were cold rolled to 95% reduction from 6mm thickness ( the diameter of the rolls was 52mm). Rolling was performed in the following way : about 1.5mm per pass to 50% reduction : 1mm to 95 percent reduction. The specimens were turned end for end between passes. In order to achieve homogeneous deformation through the specimen special attention was given to keep the ratio of the length of the rolls to specimen thickness larger than 1 (8).

$$l_c / d > 1 \quad (l_c \cong (R \cdot \Delta d)^{1/2})$$

Broadening was avoided by a ratio of specimen broadness to thickness  $b/d > 3$ . This led to a homogeneous stress state which nearly fulfills the conditions of an ideal plane strain compression. In order to avoid orientation gradients, the specimens were thinned from both faces by mechanical polishing to approximately 0.25mm thick

**Table1. The Relation between Axial  
Motion Data Aquisition**

<b>Large Degree (o/mm) Scale level</b>	<b>Small Degree (o/mm) Scale level</b>	<b>Pitch per Rotation Rotation Step</b>	<b>Number of Data</b>	<b>Data Aquisition (timer)</b>
<b>1  12<sup>0</sup>/16</b>	<b>right 435/8</b>	<b>5</b>	<b>1296</b>	<b>5.555</b>
		<b>5</b>		
	<b>left 435/16</b>	<b>5</b>	<b>2592</b>	<b>2.777</b>
		<b>2.5</b>		
<b>2  6<sup>0</sup>/16</b>	<b>right 435/8</b>	<b>2.5</b>	<b>2592</b>	<b>5.555</b>
		<b>5</b>		
	<b>left 435/16</b>	<b>2.5</b>	<b>5184</b>	<b>2.777</b>
		<b>2.5</b>		

Table 2. Setting of  $2\theta$ 

	pole material	$a\text{\AA}$	111	200	220
Cu Tube $\lambda = 1.54\text{\AA}$	Cu	3.6148	43.39	50.39	74.26
	Ag	4.0779	38.18	44.38	64.56
	LiF	4.027	38.68	44.97	65.48
	Al	4.0497	38.46	44.70	65.07
	Cu 5% Ag	3.624	43.19	50.29	73.88
	Cu 2.5% Ag	3.624	43.29	50.42	74.09
Mo Tube $\lambda = 0.71\text{\AA}$	Cu		19.59	22.65	32.25
	Ag		17.34	20.05	28.51
	LiF		16.56	20.31	28.88
	Al		17.47	22.20	28.72
	Cu 5% Ag		19.54	22.60	32.17
	Cu 2.5% Ag		19.58	22.65	32.24

### 3.2.2 Heat Treatment of the samples

For the rolling textures two types of heat treatment were carried out. These heat treatment schedules are summarized in Figure 18. The first was used to study the recrystallization behavior of a supersaturated  $\alpha$  solid solution. It was annealed at  $900^{\circ}\text{C}$  for 7 hours, followed by water quenching. The second was designed to investigate the rolling and annealing texture development of the two phase material ( $\alpha$  solid solution +  $\beta$  solid solution) and accomplished by annealing at  $600^{\circ}\text{C}$  for three hours and then cooled by water quenching.

In order to determine the recrystallization temperature isochronal tests were carried out on both solid solution and two phase material, cold rolled to 95% reduction. The results are plotted as 'isochronal curve' in Figure 19. The major drop in hardness is due to the recrystallization, which occurs between  $525$  and  $575^{\circ}\text{C}$  in the solid solution sample while a similar drop occurs between  $575$  and  $625^{\circ}\text{C}$  for the two phase material.

The copper-silver phase diagram indicates that the copper alloy containing 5% silver will be in  $\alpha$  solid solution between  $780^{\circ}\text{C}$  and  $980^{\circ}\text{C}$ . Below  $780^{\circ}\text{C}$  the solubility of silver in copper is less than 5%. Thus, if the alloy is maintained for three hours back up to  $650^{\circ}\text{C}$  after quenching from homogenizing temperature,  $\beta$  solid solution to precipitate.

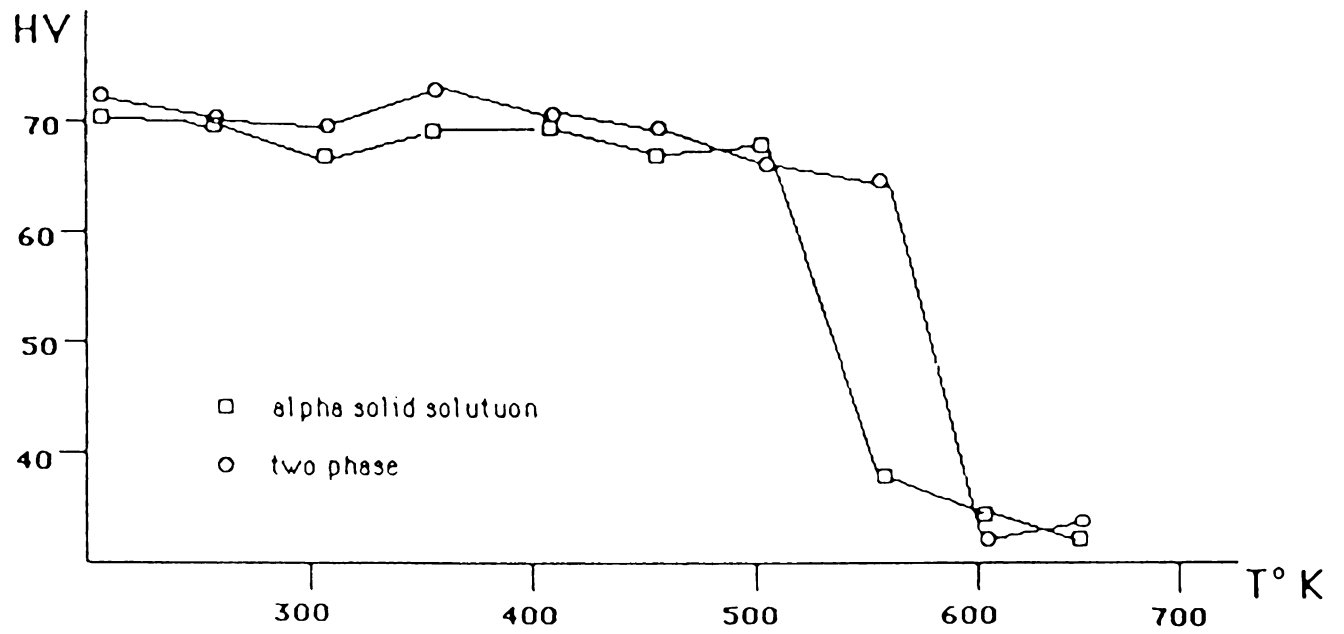


Figure 19 : Hardness variation during annealing of rolled specimens.

## CHAPTER 4

### RESULTS AND DISCUSSION

#### 4.1 Rolling Texture

##### 4.1.1 Experimental Results

Textures were obtained from both (111) and (200) reflections by using the Schulz reflection method. Complete pole figures were then obtained by normalizing all data with respect to the random powder specimen.

The Cu-Ag alloy (solid solution) rolled to 95% reduction exhibits a brass type texture which is superimposed by the brass- and goss- position. These two texture components are presented clearly by the {111} and {200} pole figures in Figure. Also the Cu-Ag alloy (two phase) rolled to 95% reduction shows a same texture composed of the brass- and goss- orientation like Cu-Ag solid solution alloy. There was no evidence to distinguish the rolling texture of the solid solution alloy from that of two phase alloy.

##### 4.1.2 Discussion

It is common to distinguish between two types of rolling textures at high rolling reduction. One is the copper- (pure metal) type texture at high stacking fault energy and the other is the brass- (alloy) type texture at low stacking fault energy. According to the present result it seems to be obvious that 5% alloy content can decrease the stacking fault energy of Cu-Ag alloy low enough. Thus the transition of the rolling texture observed here for the Cu-Ag alloy is similar to that observed in the brass and Cu-P alloy (10). Only the amount of alloy content to cause the transition was different in such a way that 5% Ag corresponds to 14% and 1% P. It shows once again that only one parameter, i.e. SFE, is supposed to cause this rolling texture transition.

Thus the mechanism of this texture formation can be explained as same as that of brass and

Cu-P alloy. In low SFE alloys slip is preferred on planes parallel to the twin boundaries of the fine twin lamella, which leads to an abnormal rotation into the  $\{323\}\langle 113 \rangle$  and the  $\{111\}\langle 110 \rangle$  positions. The formation of shear bands through these rotated twin regions changes their orientations again to near the goss- and brass- position forming the final brass type rolling texture, (16).

## 4.2 Recrystallization Texture

### 4.2.1 Experimental Results

The recrystallization textures of the Cu-Ag solid solution alloy after rolling and annealing at 600 C composes of three main components, the goss-, cube-, and  $\{258\}\langle 121 \rangle$ -orientation (about  $37^\circ\langle 100 \rangle$  orientation relationship to the brass- component). If annealed at 550 C, this alloy shows a different texture which is composed of cube- and  $\{258\}\langle 121 \rangle$ -component. Obviously some influence is exerted by the annealing temperature, since the texture annealed at 600 C reveals a goss-component in addition to two components present at 550 C. These pole figures are shown in Figure.

For the Cu-Ag two phase alloy the recrystallization texture is composed of the goss orientation and  $\{258\}\langle 121 \rangle$  (near brass) position occurs. This is shown in Fig. .

### 4.2.2 Discussion

In the present work, different preannealings influenced the temperature of recrystallization and the textures practically.

After primary recrystallization one find relatively different textures for Cu-Ag solid solution alloy and for Cu-Ag two phase alloy. In first case the resulting textures are varying according to the annealing temperature. While the brass component of rolling disappears the goss component still shows the strong intensity. Thus retained goss component can be explained by the nucleation based on the subgrain growth. And the component  $\{258\}\langle 121 \rangle$  which has an  $37^\circ\langle 100 \rangle$  orientation relationship to the brass component as in case of Cu-P alloy (16). And the



component  $\{258\}\langle 121 \rangle$  seems to be due to the preferred high growth rate. However the origin of the cube component is unknown.

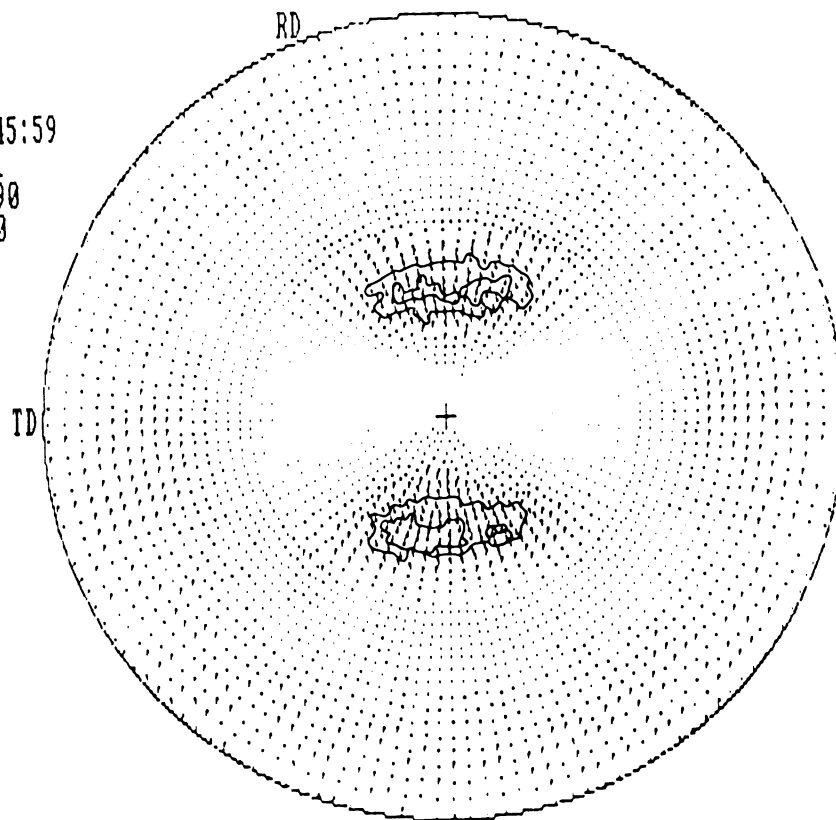
It can be pointed out that there should be some interaction between recrystallization and the precipitations from the different annealing textures according to different temperatures. Thus the resultant recrystallization texture were influenced to some extent by the temperature and time of annealing. At present, however it is impossible to formulate the conditions to produce this difference.

In second case both the goss position and  $\{011\}\langle 733 \rangle$  position (near the brass component) are strong similar to the rolling texture. These have a certain similarity to the rolling texture besides the brass component of rolling is rotated about  $10^\circ$  around its  $\langle 110 \rangle$ . One can assume that the small amount of excess  $\beta$  solid solution along the grain boundaries cause the retention and the slight rotation of the brass component. The goss component is again seems to be nucleated by subgrain growth.

POLE FIGURE  
 ^^^^^^^^^^^^^^^

01-30-1986 00:45:59  
 FILE NAME : 26.111  
 REFL. : FROM 90  
 TO 0  
 H K L : 111  
 ANODE : CU  
 PITCH : 2.5  
 ROT. STEP : 2.5

DEN	X*RANDOM
0	0.285
1	0.634
2	0.983
3	1.333
4	1.682
5	2.031
6	2.380
7	2.730



POLE FIGURE  
 ^^^^^^^^^^^^^^^

01-30-1986 00:52:06  
 FILE NAME : 26.200  
 REFL. : FROM 90  
 TO 0  
 H K L : 200  
 ANODE : CU  
 PITCH : 2.5  
 ROT. STEP : 2.5

DEN	X*RANDOM
0	0.187
1	0.593
2	0.998
3	1.404
4	1.809
5	2.215
6	2.620
7	3.026

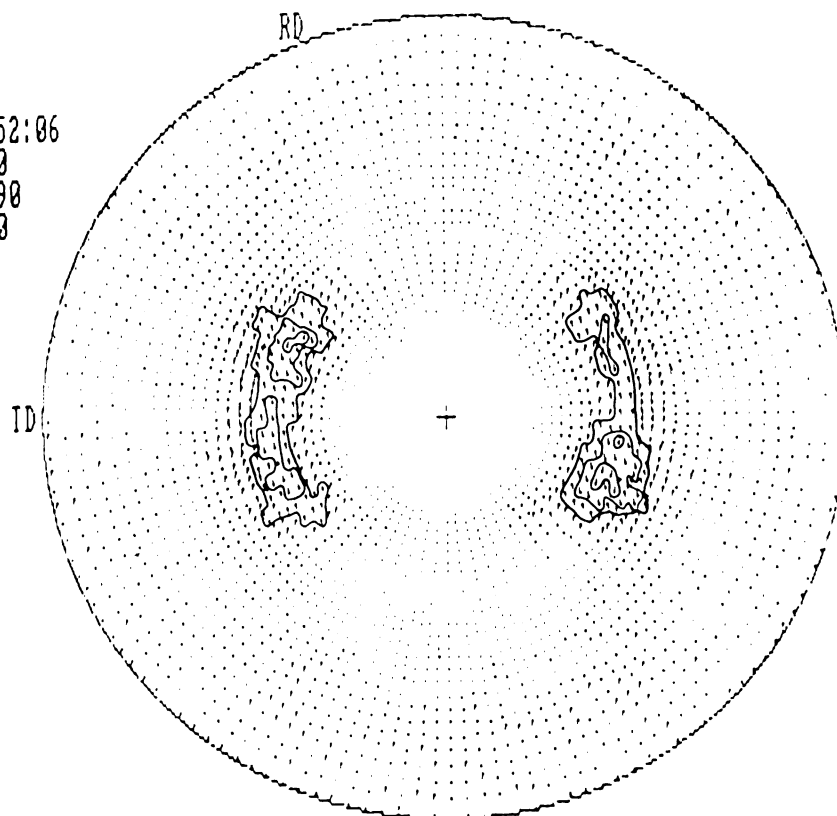


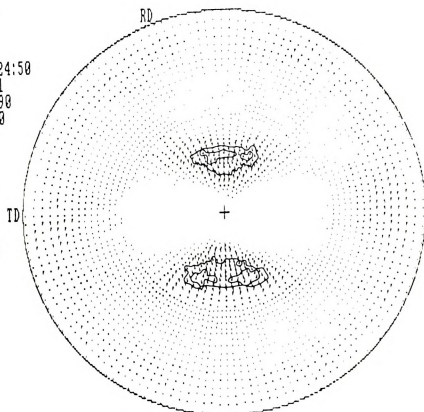
Figure 20 - (111), (200) pole figures for Cu-5%Ag (solid solution) rolled to 95% reduction at room temperature.



POLE FIGURE  
AAAAAAAAAAAA

01-30-1986 00:24:50  
 FILE NAME : 34.111  
 REFL. : FROM 90  
 TO 0  
 H K L : 111  
 ANODE : CU  
 PITCH : 2.5  
 ROT. STEP : 2.5

DEN X\*RANDOM  
 0 0.146  
 1 0.566  
 2 0.985  
 3 1.404  
 4 1.824  
 5 2.243  
 6 2.662  
 7 3.081

POLE FIGURE  
AAAAAAAAAAAA

01-30-1986 00:37:26  
 FILE NAME : 34.200  
 REFL. : FROM 90  
 TO 0  
 H K L : 200  
 ANODE : CU  
 PITCH : 2.5  
 ROT. STEP : 2.5

DEN X\*RANDOM  
 0 0.170  
 1 0.652  
 2 1.135  
 3 1.618  
 4 2.101  
 5 2.584  
 6 3.067  
 7 3.550

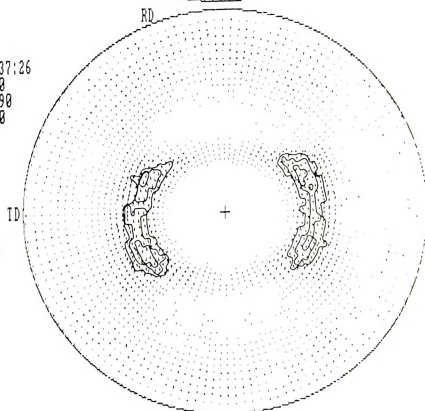
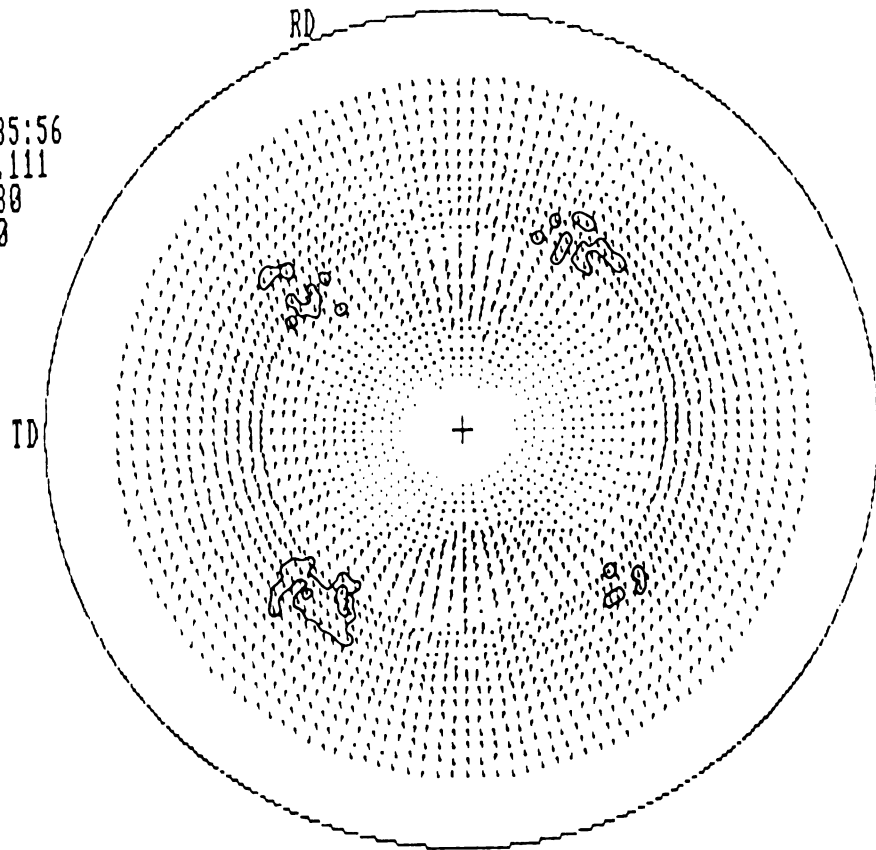


Figure 21 : (111), (200) pole figures for Cu-5%Ag (two phase alloy) rolled to 95%  
 reduction at room temperature

POLE FIGURE  
 ^^^^^^^^^^^^^^^  
 02-01-1986 19:35:56  
 FILE NAME : 17550.111  
 REFL. : FROM 80  
 TO 0  
 H K L : 111  
 ANODE : CU  
 PITCH : 2.5  
 ROT. STEP : 2.5

DEN	X*RANDOM
0	0.107
1	0.321
2	0.535
3	0.749
4	0.963
5	1.177
6	1.391
7	1.605



POLE FIGURE  
 ^^^^^^^^^^^^^^^  
 02-01-1986 19:46:36  
 FILE NAME : 17550.200  
 REFL. : FROM 80  
 TO 0  
 H K L : 200  
 ANODE : CU  
 PITCH : 2.5  
 ROT. STEP : 2.5

DEN	X*RANDOM
0	0.000
1	0.272
2	0.544
3	0.816
4	1.088
5	1.360
6	1.632
7	1.903

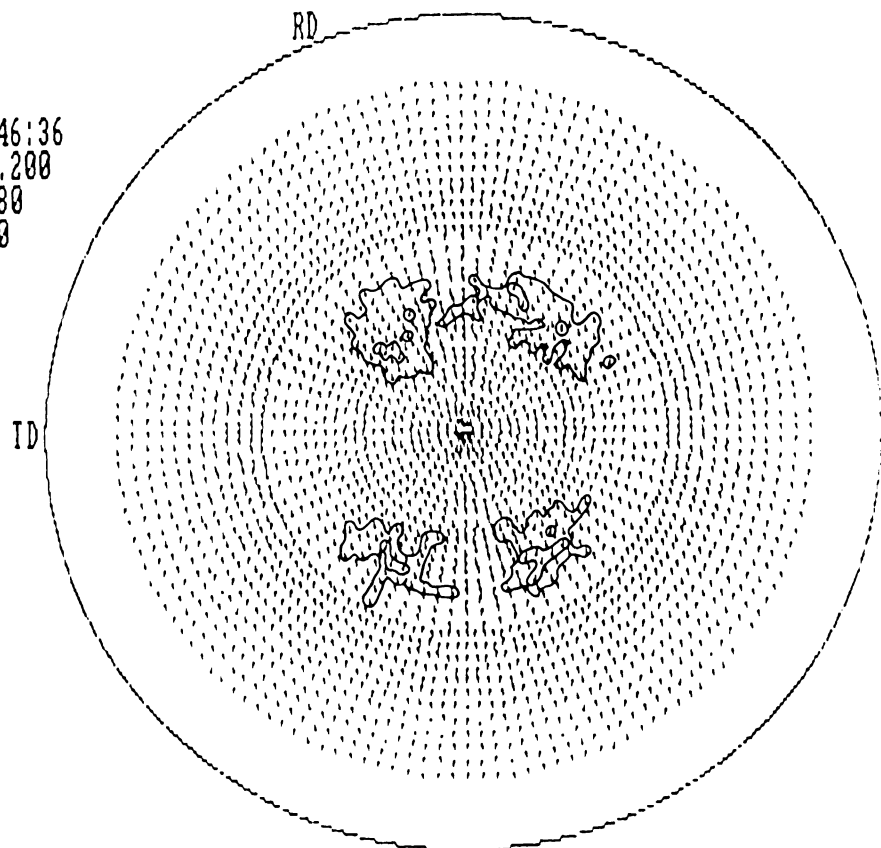
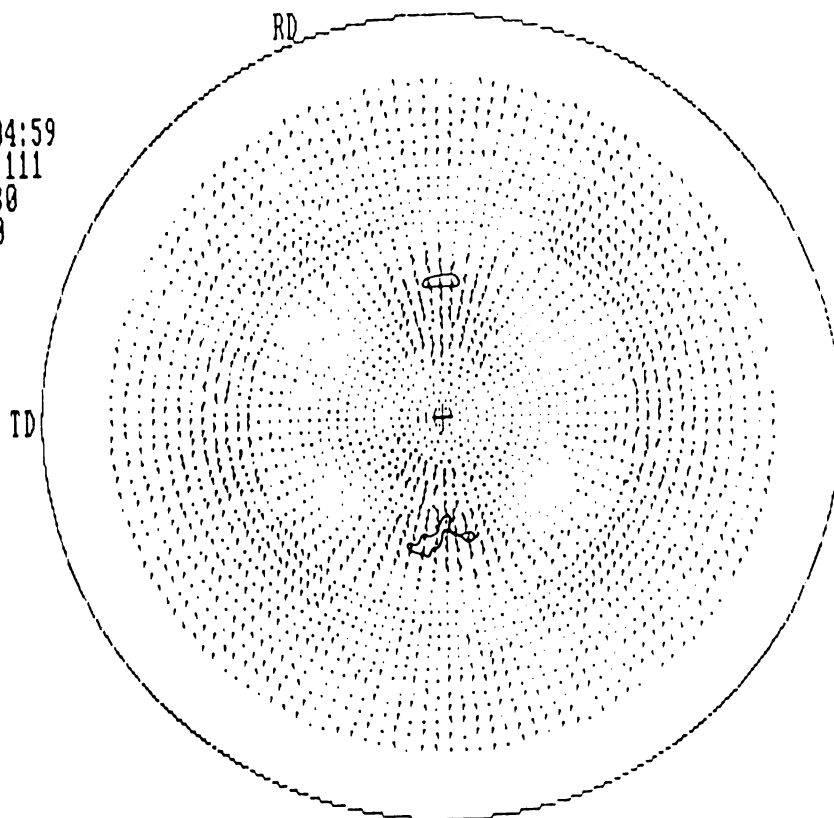


Figure 22-1 (111),(200) pole figures of recrystallization textures of Cu-5%Ag solid solution alloy after rolling and annealing at 550°C.

POLE FIGURE  
 ^^^^^^^^^^^^^^^  
 02-01-1986 20:04:59  
 FILE NAME : 26600.111  
 REFL. : FROM 80  
 TO 0  
 H K L : 111  
 ANODE : CU  
 PITCH : 2.5  
 ROT. STEP : 2.5

DEN	X*RANDOM
0	0.722
1	0.854
2	0.985
3	1.116
4	1.247
5	1.379
6	1.510
7	1.641



POLE FIGURE  
 ^^^^^^^^^^^^^^^  
 02-01-1986 20:20:38  
 FILE NAME : 26600.200  
 REFL. : FROM 80  
 TO 0  
 H K L : 200  
 ANODE : CU  
 PITCH : 2.5  
 ROT. STEP : 2.5

DEN	X*RANDOM
0	0.681
1	0.848
2	1.015
3	1.182
4	1.349
5	1.515
6	1.682
7	1.849

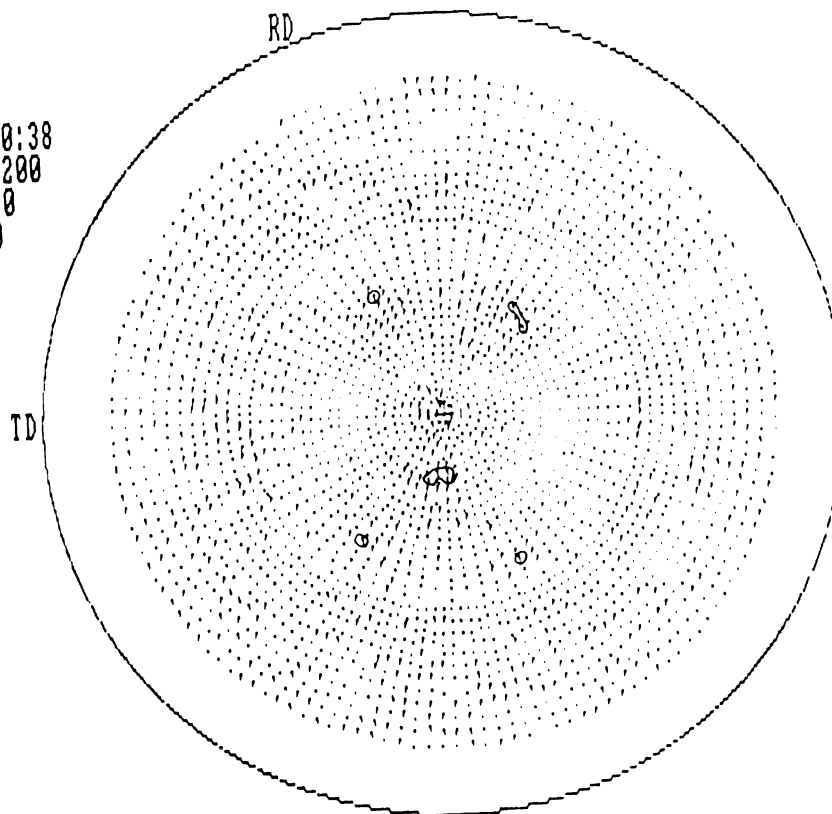
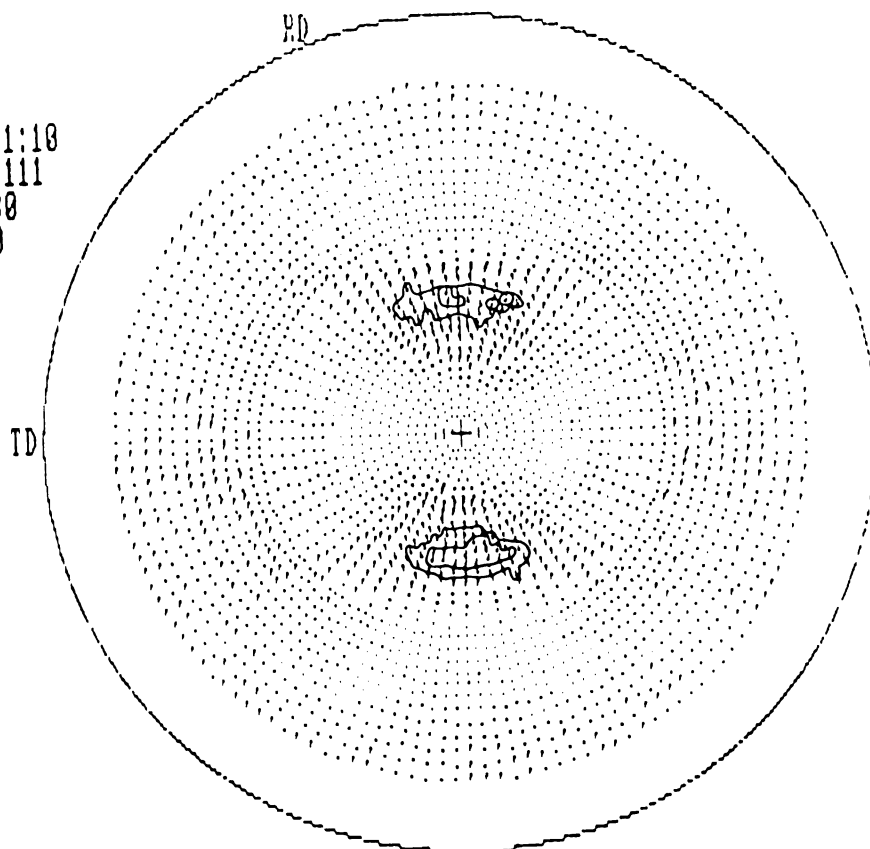


Figure 22-2 - (111), (200) pole figures of recrystallization textures of Cu-53Ag solid solution alloy after rolling and annealing at 600°C.

POLE FIGURE  
 ^^^^^^^^^^^^^^^  
 02-01-1986 20:31:18  
 FILE NAME : 33600.111  
 REFL. : FROM 80  
 TO 0  
 H K L : 111  
 ANODE : CU  
 PITCH : 2.5  
 ROT. STEP : 2.5

DEN	X*RANDOM
0	0.013
1	0.390
2	0.767
3	1.144
4	1.521
5	1.898
6	2.275
7	2.651



POLE FIGURE  
 ^^^^^^^^^^^^^^^  
 02-01-1986 20:39:26  
 FILE NAME : 33600.200  
 REFL. : FROM 80  
 TO 0  
 H K L : 200  
 ANODE : CU  
 PITCH : 2.5  
 ROT. STEP : 2.5

DEN	X*RANDOM
0	0.518
1	0.720
2	0.922
3	1.124
4	1.326
5	1.528
6	1.729
7	1.931

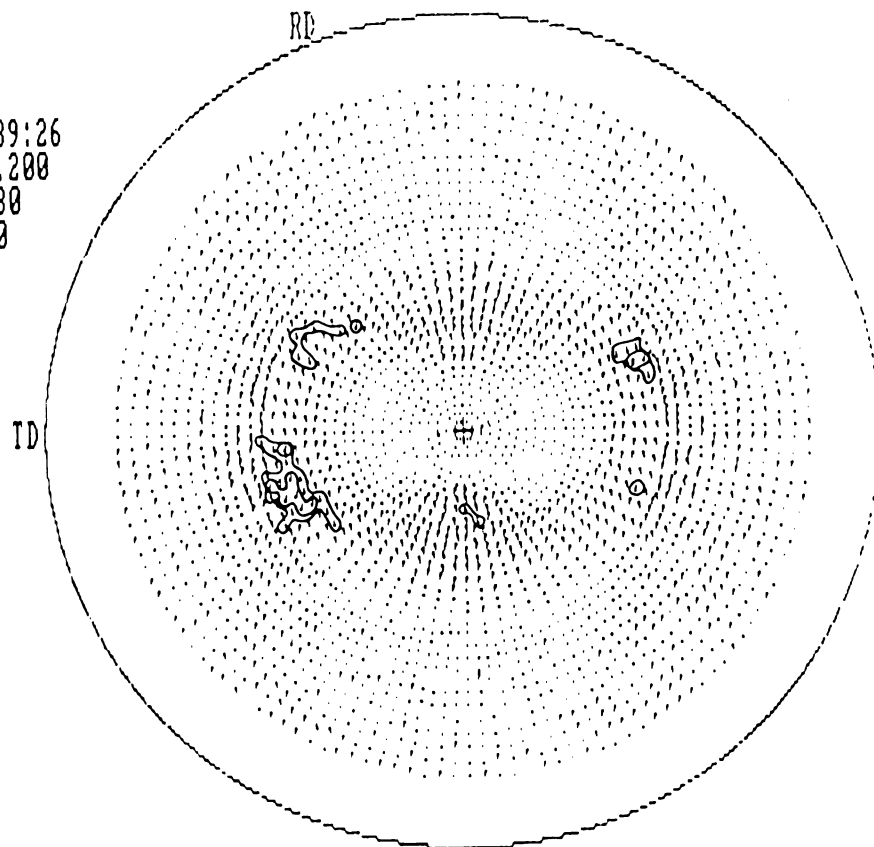


Figure 23. (111), (200) pole figures of recrystallization textures of Cu-5%Ag two phase alloy after rolling and annealing at 600°C

## CHAPTER 5

### SUMMARY AND CONCLUSIONS

In the present paper textures were obtained from both (111) and (200) reflections by using the Schulz reflection. Complete pole figures were then obtained by normalizing all data with respect to the random powder specimen.

The transition of the rolling texture observed here for both the Cu-Ag solid solution alloy and the Cu-Ag two phase alloy is similar to that observed in the brass and Cu-p alloy. Only the amount of alloy content to cause the transition was different. It shows again that only one parameter, i.e. SFE, is supposed to cause this rolling texture transition.

After primary recrystallization one finds relatively different textures for the Cu-Ag solid solution alloy and for the Cu-Ag two phase alloy. In first case the resulting textures are not brass recrystallization textures and are varying according to the annealing temperatures. In second case the resultant textures have a certain similarity to the rolling textures besides the brass component of rolling is rotated about  $10^\circ$  around its  $\langle 110 \rangle$ . The recrystallization textures depend first on the rolling textures which is determined by the SFE. Secondly it depends on precipitates along the grain boundary. These complicated dependencies are the reason for the variety of recrystallization textures as compared to rolling textures.



## BIBLIOGRAPHY

1. G.WASSERMANN, J.GREWEN, Texturen metallischer Werkstoffe, Springer-verlag, Berlin/Göttingen/Heidelberg (1962).
2. R.ALAM, H.D.MENDELBERG, and K. LUCKE, Z.Metallkunde 58 (1967) 867.
3. G.WASSERMANN, Z.Metallkunde 54(1963) 61.
4. H.MECKING, Int. Conf. on Textures, Vol. 1, Tokyo (1981) 57.
5. H.HONEFF, H.MECKING, INT. Conf. on Textures, Vol. 1, Aachen (1978) 265.
6. H.MECKING, Int. Conf. on Textures, Vol. 1, Aachen (1978) 25.
7. G.GOTTSTEIN, Int. Conf. on Textures, Vol. 1, Aachen (1978) 96.
8. P.A.BECK, Acta Met., 1(1953) 230.
9. B.LIEBMANN, K.LUCKE, and G.MASING, Z.Metallkunde 47 (1956) 57.
10. U.SCHMIDT, K.LUCKE, and J.POSPIECH, Int. Conf. on Textures, Cambridge (1975) 154.
11. H.J.BUNGE, K.H.PUCH, Z.Metallkunde 75(1984) 124.
12. L.G.SCHULZ, J.Appl.Phys. 20(1949) 1030.
13. H.J.BUNGE Texture Analysis in Materials Science, Butterworth, London (1982) 92.
14. E.A.OWEN, J.ROGERS, J.Inst.Met. 57 (1935) 257.
15. K.LUCKE, Int. Conf. on Texture, Vol. 1, Tokyo (1981) 14.
16. J.HIRSCH, K.VIRNICH, and K.LUCKE, Int Conf. on Textures, vol. 1, Tokyo (1981) 375.

MICHIGAN STATE UNIVERSITY LIBRARIES



3 1293 03062 2637